Running Title: Estrogen-driven WNT4 signaling

Research article

Estrogen controls mTOR signaling and mitochondrial function via WNT4 in lobular carcinoma

Deviyani M. Rao[1], Evelyn K. Bordeaux[1], Hannah M. Hicks[1], Steffi Oesterreich[2], Matthew J. Sikora[1]

Affiliations

[1]Dept. of Pathology, University of Colorado Anschutz Medical Campus

[2]Women's Cancer Research Center, Dept. of Pharmacology and Chemical Biology, UPMC Hillman Cancer Center

Corresponding author

Matthew J. Sikora, PhD.; Mail Stop 8104, Research Complex 1 South, Room 5117, 12801 E. 17th Ave.; Aurora, CO 80045. Tel: (303)724-4301; Fax: (303)724-3712; email: matthew.sikora@ucdenver.edu. Twitter: @mjsikora

Authors' contributions

MJS, DMR, and SO conceived of the project and experiments. MJS, DMR, EKB, and HMH designed and performed experiments. MJS and DMR developed models for the project. All authors contributed to data analysis and interpretation. MJS wrote the draft manuscript; all authors read and revised the manuscript and have read and approved of this version of the manuscript.

Key words

WNT4, Wnt signaling, estrogen, estrogen receptor, breast cancer, lobular carcinoma, mTOR, MCL1

Competing interests

The authors have nothing to disclose.

Funding

This work was supported by R00 CA193734 (MJS) from the National Institutes of Health, and by a grant from the Cancer League of Colorado, Inc (MJS). EKB is supported by T32 GM007635. SO's work on ILC is supported by Susan G. Komen Leadership grant (SAC160073) and a Breast Cancer Research Foundation grant. This work utilized U. Colorado Cancer Center Shared Resources supported by P30 CA046934.

Data availability

Data associated with experiments herein will be available at an Open Science Framework repository [1] (https://doi.org/10.17605/OSF.IO/7X8NG) upon publication, or upon request.

Abstract

Invasive lobular carcinoma of the breast (ILC) is strongly estrogen-driven, and represents a unique context for estrogen receptor (ER) signaling. In ILC, ER controls the expression of the Wnt ligand WNT4, which is critical for endocrine response and anti-estrogen resistance, yet signaling mediated by WNT4 is poorly understood. We utilized reverse phase protein array (RPPA) to characterize ER and WNT4-driven signaling in ILC cells, and identified WNT4 as a mediator of downstream mTOR signaling via p70-S6K. Independent of mTOR/p70-S6K, ER and WNT4 control levels of MCL-1, which is associated with mitochondrial function. In this context, knockdown of WNT4 caused accumulation of reactive oxygen species and decreased ATP production that precede cell death. WNT4 regulation of both mTOR signaling and MCL-1 levels was also observed in anti-estrogen resistant models of ILC. Further, we identified that high *WNT4* expression is associated with similar mTOR pathway activation in serous ovarian cancer tumors, suggesting that this WNT4 pathway is important in multiple tumor types. The identified downstream pathways represent potential targets to inhibit WNT4 signaling in ovarian cancer and overcome anti-estrogen resistance for patients with ILC.

Introduction

Invasive lobular carcinoma of the breast (ILC), the second most common histologic subtype of breast cancer [2–4], appears to be exquisitely sensitive to and dependent on the steroid hormone estrogen. Estrogen-based hormone replacement therapy (with or without progestin) more strongly increases the incidence of ILC versus the more common invasive ductal carcinoma (IDC)(reviewed in [3]), and nearly all ILC tumors express ER [4–6]. Further, ILC biomarkers are consistent with the hormone-dependent 'Luminal A' molecular subtype [4], supporting the current paradigm that patients with ILC are ideal candidates for treatment with anti-estrogen therapies. However, retrospective studies suggest patients with ILC may not receive similar benefit from anti-estrogens as patients with IDC, ie. poorer outcomes with adjuvant tamoxifen [7, 8] and poorer long-term outcomes >5-10 years post-diagnosis [9–12]. Consistent with clinical observations, we identified tamoxifen-resistance in ER-positive ILC models, including *de novo* ER partial agonism by anti-estrogens [13, 14]. These data raise the question of whether ER function and signaling is unique in the context of ILC.

Studies using laboratory models of ILC and tumor profiling through the Cancer Genome Atlas support that some aspects of ER signaling are distinct in ILC versus IDC cells. TCGA analyses [4] specifically compared Luminal A ILC to Luminal A IDC, and reverse-phase protein array (RPPA) data identified differential activity of PTEN and downstream Akt signaling. Additionally, each of the three transcriptional subtypes of ILC (Reactive, Immune, and Proliferative) showed distinct signaling features in RPPA analyses (eg. high c-kit; high STAT5; high DNA repair protein signature; respectively). Similarly, we reported that ER regulates unique target genes in ILC cells via distinct ER DNA binding patterns [13]. These unique targets mediate ILC-specific signaling pathways driven by ER that are critical for endocrine response and resistance, eg. estrogen-driven atypical Wnt signaling via WNT4 [15, 16]. However, our understanding of ER-driven signaling at the protein level in ILC cells remains limited, as studies to date either cannot define dynamic changes caused by ER activation (ie. are from static samples as in TCGA), or are focused on the ER-driven transcriptome. Proteomic studies in ILC with estrogen or anti-estrogen treatment are needed to better understand ER-driven signaling in ILC.

We identified WNT4 as a critical signaling molecule induced by ER specifically in ILC, but the mechanism by which WNT4 engages downstream signaling is unknown. WNT4 is unique among Wnt proteins in its diverse roles in either activating or suppressing canonical or non-canonical Wnt signaling in a tissue-specific manner (discussed in [16]). In the normal mammary gland, WNT4 is induced by progesterone in progesterone receptor (PR)-positive luminal epithelial cells, then secreted to act in a paracrine manner to activate canonical β-catenin-dependent signaling in neighboring myoepithelial

cells [17–20]. In contrast, WNT4 is under direct control of ER, not PR, in ILC cell lines [13, 15]. Canonical Wnt signaling is also dysfunctional in ILC cells; hallmark genetic loss of E-cadherin (*CDH1*) causes catenin protein dysfunction including destabilization and loss of β-catenin protein in both cell lines and tumors [4, 15]. Further, we recently reported that WNT4 secreted from ILC cells (and other cancer models) is dysfunctional for paracrine activity, but instead activates signaling by a cell-autonomous, intracellular mechanism (ie. “atypical” Wnt signaling [16]). Taken together, defining ER-driven signaling and novel WNT4-driven signaling in ILC is necessary to both understand ILC biology and identify new treatment targets for ILC.

To address these gaps in our understanding of ER function in ILC, we used RPPA analyses of ILC models to characterize ER-driven signaling in ILC, and to determine the role of WNT4 in mediating ER-driven signaling. These studies identified that estrogen activates distinct protein signaling pathways in ILC cells, including a distinct component of PI3K/Akt/mTOR signaling in ILC versus IDC cells. A subset of ER-driven signaling in ILC cells required WNT4, most notably mTOR activity and regulation of mitochondrial function. These observations led us to further examine the mechanisms by which ER-driven WNT4 signaling mediates cell proliferation and survival, and endocrine response and resistance, in ILC cells.

Materials and Methods

Cell culture

MDA MB 134VI (MM134) and SUM44PE (44PE) were maintained as described [13]. MCF-7 and HCC1428 were maintained in DMEM/F12 (Corning Life Sciences, cat#10092CV) supplemented with 10% fetal bovine serum (FBS; Nucleus Biologics, cat#FBS1824). Hormone-deprivation was performed as described [21] in IMEM (Gibco/ThermoFisher, cat#A10488) supplemented with 10% charcoal-stripped fetal bovine serum (CSS; prepared as described [21] with the same FBS as above). WNT4-overexpressing models were previously described [16], and cultured in the same conditions as parental cell lines. Long-term estrogen deprived (LTED) model establishment and culture conditions were previously described [15]. All lines were incubated at 37°C in 5% CO_2. Cell lines are authenticated annually via the University of Arizona Genetics Core cell line authentication service and confirmed to be mycoplasma negative every four months. Authenticated cells were in continuous culture <6 months.

17β-Estradiol (E2; cat#2824) and fulvestrant (fulv / ICI182,780; cat#1047) were obtained from Tocris Bioscience and dissolved in ethanol. Everolimus (ever; cat#11597), PF-04708671 (PF; cat#15018), ABT199 (cat#16233), ABT263 (cat#11500), WEHI539 (WEHI; cat#21478), and A1210477 (A121; cat#21113) were obtained from Cayman Chemical and dissolved in DMSO.

RNA interference

siRNAs were reverse transfected using RNAiMAX (ThermoFisher) according to the manufacturer's instructions. All constructs are siGENOME SMARTpool siRNAs (Dharmacon/Horizon Discovery): Non-targeting pool #2 (D-001206-14-05), Human *WNT4* (M-008659-03-0005), Human *FOXM1* (M-009762-00-0005), Human *MCL1* (M-004501-08-0005), Human *CDKN1A* (M-003471-00-0005). Details regarding validation of the specific effects of the *WNT4* siRNA pool are previously described [15].

Reverse phase protein array (RPPA)

Cells were hormone-deprived prior to reverse transfection with 10nM siRNA as described above. 24 hours post-transfection, cells were treated with vehicle (0.01% EtOH) or 100pM E2 and harvested 24 hours later (48h post-transfection; 24h post-treatment). Cells were lysed according to core facility instructions (see below, [22]). Briefly, cells were washed twice with cold PBS, and incubated on ice with 60µL of RPPA lysis buffer (see below) for 20'. Lysates were collected by scraping and centrifuged at ~16,000xg at 4°C for 10'. Supernatant was collected and utilized for RPPA analyses. RPPA lysis buffer was made with 1% Triton X-100, 50mM HEPES (pH 7.4), 150mM NaCl, 1.5mM $MgCl_2$, 1mM EGTA,

and 10% glycerol, supplemented with Halt Protease and Phosphatase Inhibitor Cocktail (Pierce/ThermoFisher, cat#78440).

RPPA analyses and data normalization were carried out by the MD Anderson Cancer Center Functional Proteomics Core Facility (August 2016; platform included 305 antibodies listed in **Supplemental Table 1**). Details for RPPA signal normalization and quality control provided by the core facility are in **Supplemental Document 1**; Normalized Linear data are presented in all analyses herein. Multiple testing correction was applied using the Benjamini–Hochberg method. Raw/normalized RPPA data and treatment comparisons will be deposited to an OSF page upon formal publication [1], or will be provided upon request.

Immunoblotting

Whole-cell lysates were obtained by incubating cells in RPPA lysis buffer (above) for 20' on ice. Cells were centrifuged at ~16,000xg for 10m at 4°C and the resulting supernatant was collected for analysis. Protein concentration was measured using the Pierce BCA Protein Assay Kit (#23225). Standard methods were used to perform SDS-PAGE. Proteins were transferred onto PVDF membranes. Antibodies were used according to manufacturer's recommendations: WNT4 (R&D, MAB4751, cat# 55025); ERα (ThermoFisher, 6F11, cat# MA1-80216); pER-S118 (Cell Signaling, 16J4, cat#2511); FOXM1 (Cell Signaling, D12D5, cat#5436); total S6 (Cell Signaling, 54D2, cat#2317); pS6-S235/236 (Cell Signaling, cat#2211); pS6-S240/244 (Cell Signaling, cat#2215); p70-S6K (Cell Signaling, 49D7, cat#2708); p-p70-S6K-T389 (Cell Signaling, 108D2, cat#9234); MCL1 (Cell Signaling, D35A5, cat#5453); 4E-BP1 (Cell Signaling, cat#9452); p4E-BP1-S65 (Cell Signaling, 174A9, cat#9456); Histone H3 (Abcam, cat#ab1791). Secondary antibodies were used according to manufacturer's instruction and were obtained from Jackson ImmunoResearch Laboratories (West Grove, PA, USA): Goat Anti-Mouse IgG (cat # 115-035-068), Goat Anti-Rabbit IgG (cat# 111-035-045) and Goat Anti-Rat IgG (cat# 112-035-062). Chemiluminescence was used to detect antibodies and either film or the LI-COR c-Digit (LI-COR Biosciences, Lincoln, NE, USA) was used to develop the immunoblots. Specific considerations regarding the use of the WNT4 antibody are described elsewhere [16]. Total protein (Ponceau) served as a loading control.

Cell proliferation and cell cycle analyses

Total double-stranded DNA was measured as a proxy for total cell number by hypotonic lysis of cells in ultra-pure H_2O, followed by addition of Hoechst 33258 (ThermoFisher Scientific, #62249) at 1µg/mL in Tris-NaCl buffer (10mM Tris, 2M NaCl; pH 7.4) at equivalent volume to lysate. Fluorescence (360nm ex

/ 460nm em) was measured on a Bio-Tek Synergy 2 microplate reader. For cell cycle analyses, cells were fixed in 70% EtOH overnight at 4°C. After fixation, cells were treated with RNase A, and stained with 50µg/mL propidium iodide + 0.1% Triton X-100 in PBS overnight at 4°C. PI intensity was assessed on a Gallios Flow Cytometer (Beckman Coulter) at the U. Colorado Cancer Center Flow Cytometry Core Facility; at least 10,000 events were counted per sample.

Quantitative PCR analyses

RNA extractions were performed using the RNeasy Mini kit (Qiagen); mRNA was converted to cDNA on an Eppendorf Mastercycler Pro (Eppendorf) and using Promega reagents: Oligo $(dT)_{15}$ primer (cat# C110A), Random Primers (cat# C118A), GoScript 5x Reaction Buffer (cat# A500D), 25mM MgCl2 (cat# A351H), 10mM dNTPs (cat# U1511), RNasin Plus RNase Inhibitor (cat# N261B) and GoScript Reverse Transcriptase (cat# A501D). qPCR reactions were performed with PowerUp SYBR Green Master Mix (Life Technologies, cat #100029284) on a QuantStudio 6 Flex Real-Time PCR system (ThermoFisher). Expression data were normalized to *RPLP0*. Primer sequences were published previously [13, 15].

Metabolic analyses

Cellular reactive oxygen species (ROS) were measured by CM-H_2DCFDA (ThermoFisher, cat#C6827) fluorescence. Cells were reverse transfected as described above, and 24h later loaded with 5µM dye per manufacturer's instructions. 24h later (ie. 48h post-transfection), fluorescence-positive cells were identified using an Incucyte Zoom live cell imaging platform (Essen Bioscience) and normalized to total cellular confluence. For analysis of ATP per cell, cells were reverse transfected as above, and at the indicated timepoint, parallel plates were assessed for total dsDNA and total ATP (Cell Titer-Glo, Promega). Cell number by each method was normalized to a standard curve, and analyzed as a ratio of (Cell Number by ATP)/(Cell Number by dsDNA).

TCGA data analyses

TCGA data were accessed via the cBio portal in March-June 2019; provisional datasets were used for all analyses described. Z-score cutoffs for *WNT4* expression (RNAseq) were selected based on the minimum z-score needed to exclude any low *WNT4*-expressing tumors. All statistical analyses were derived from cBio analysis tools, ie. Enrichments>Protein>RPPA.

Results

Estrogen activates a distinct subset of PI3K-mTOR related signaling in ILC cells

We profiled estrogen-driven signaling by RPPA, comparing hormone-deprived cells treated with vehicle (0.01% EtOH) vs 1nM E2 for 24hrs. ILC cell lines MDA MB 134VI (MM134) and SUM44PE (44PE) were compared to IDC cell line MCF-7 (**Figure 1A**). Consistent with canonical pathways activated by ER, induction of ER target MYC along with other cell cycle proteins was observed in all three cell lines (**Figure 1B**). Other shared ER targets included activation of PI3K pathway proteins (eg. phospho-p70-S6K, phospho-S6-S235/S236), and suppression of caspase 7 cleavage. We also identified 18 proteins regulated by ER in MM134 and 44PE, but not in MCF-7 (ie. ILC-specific ER targets) (**Figure 1C**), mainly representing either PI3K-related signaling (eg. phospho-S6, phospho-mTOR, total MCL1) or transcriptional control (eg. NOTCH, SNAI1; we reported ER regulation of SNAI1/SNAIL previously [23]). Of note, estrogen suppressed total histone H3 in ILC (and two H3 post-translational modifications, reflective of the total H3 change). This represents a decrease in the pool of soluble non-nucleosomal H3, consistent with chromatin remodeling [24–27], rather than a change in total cellular H3 (**Supplemental Figure 1**, also see RPPA lysis conditions in Materials and Methods).

Since ILC-specific E2-regulated targets were primarily related to PI3K-mTOR signaling, we examined all PI3K-related proteins on the RPPA that were changed by E2 treatment in any cell line (**Figure 1D**) to identify components of the signaling cascade in ILC. Based on the observed estrogen-induced phosphorylation of mTOR, p70-S6K (RPS6KB1), and S6 in ILC cells (**Figure 1**), we expected to see an upstream increase in phosphorylated Akt [28]. However, estrogen-induced Akt phosphorylation was only observed in MCF-7 (**Figure 1D**), and levels of phospho- and total Akt were extremely low in ILC cells (**Figure 1E**). Additionally, Akt-mediated phosphorylation of PRAS40 was only induced by estrogen in MCF-7, not in ILC cells, suggesting mTOR activation is mediated by another pathway in ILC cells.

Since non-canonical Wnt signaling has previously been linked to Akt-independent mTOR activation [29], we further investigated the role of WNT4 in estrogen-regulated signaling and mTOR activity in ILC cells. We compared hormone-deprived ILC cells treated with estrogen (as above) transfected with non-targeting versus *WNT4*-targeting siRNA (siNT vs siWNT4, respectively). Estrogen-regulation of WNT4 and siWNT4 efficacy were confirmed by western blot (**Figure 2A**). Consistent with the critical role of WNT4 in ILC cell proliferation and survival [15], siWNT4 broadly dysregulated overall signaling (**Supplemental Figure 2A-B**). We compared siWNT4-mediated signaling changes to estrogen-regulated signaling in ILC cells, and identified 9 targets for which estrogen-regulated changes were ablated by WNT4 knockdown (**Figure 2B**). WNT4 knockdown blocked estrogen-mediated FOXM1

induction, S6 phosphorylation, MCL1 depletion, and soluble Histone H3 depletion in ILC cells; siWNT4 also increased phospho-ER (consistent with relieved negative feedback from mTOR signaling [30]). siWNT4 did not have similar effects on these targets in IDC cell lines MCF-7 or HCC1428 (**Figure 2C, Supplemental Figure 2C**). HCC1428 expresses high *WNT4* mRNA similar to that observed in ILC cell lines but does not depend on WNT4 for proliferation or survival [15], supporting that the identified signaling targets represent ILC-specific WNT4 signaling. Based on these data, we hypothesized that WNT4 mediates ILC cell proliferation and survival via regulation of FOXM1 and mTOR.

FOXM1 is not a direct target of WNT4 signaling

FOXM1 is a critical mediator of estrogen-driven cell cycle progression [31], has been linked to control of ER-driven transcription (in MCF-7 cells), and is a potential driver of anti-estrogen resistance [31–33]. This led us to examine whether FOXM1 is a critical WNT4 signaling target. Though *FOXM1* siRNA suppressed the proliferation of MM134 cells (**Supplemental Figure 3A**), this growth suppression was not equivalent to that observed with anti-estrogens or with *WNT4* siRNA. Whereas siWNT4 parallels treatment with fulvestrant and causes a G1 arrest, siFOXM1 causes a G2/M arrest (**Supplemental Figure 3B-C**), consistent with established roles of FOXM1 in progression through mitosis [34]. This lack of phenocopy between siWNT4/anti-estrogen and siFOXM1 suggested that decreased FOXM1 levels upon WNT4 knockdown may be indicative of knockdown-induced cell cycle arrest, rather than identifying FOXM1 as a direct WNT4 target. To confirm this, we examined whether CDKN1A/p21 knockdown, which partially restores proliferation after siWNT4 in ILC cells [15], would restore FOXM1 levels (ie. since p21 knockdown partially releases the G1 arrest, FOXM1 levels would increase despite WNT4 knockdown). In both MM134 and 44PE, siCDKN1A partially restored the FOXM1 decrease caused by siWNT4 (**Supplemental Figure 3D**), supporting that FOXM1 protein level is acting as a marker of cell cycle and G2/M progression. Consistent with a lack of a direct role in WNT4-driven cell cycle progression, we also did not observe any suppression of ER-driven transcription in MM134 by siFOXM1 (**Supplemental Figure 3E**). These data suggest that FOXM1 is not a direct target of ER and WNT4 in ILC, but is an indirect target of ER/WNT4-driven cell cycle progression.

WNT4 regulates mTOR signaling downstream of mTOR kinase activity

Our RPPA data showed estrogen treatment of ILC cells led to activation of mTOR activity (e.g. 4EBP1, p70S6K, and S6 phosphorylation), but siWNT4 specifically reduced S6 phosphorylation without altering p70S6K phosphorylation (T389). We confirmed via immunoblotting that targeting ER, but not WNT4, reduced p70S6K-pT389; this phosphorylation was mTOR-dependent, as treatment with everolimus completely blocked T389 phosphorylation (**Figure 3A**). Subsequent phosphorylation of S6 was reduced

by siWNT4 or by inhibiting ER, mTOR, or p70S6K (S6K1 inhibitor PF-04708671 [35]). These data suggest that WNT4 mediates S6K1 activity downstream of mTOR phosphorylation of S6K1. Consistent with this, WNT4 over-expression modestly delayed the loss of S6K1 and S6 phosphorylation caused by everolimus treatment, but ultimately downstream mTOR signaling was completely suppressed by everolimus (**Figure 3B**). WNT4 over-expression in either MM134 or 44PE did not change the effect of everolimus on cell proliferation (**Figure 3C**). Notably, though WNT4 knockdown strongly suppresses proliferation of both MM134 and 44PE, these models were resistant vs sensitive, respectively, to treatment with single-agent everolimus. Taken together, WNT4 is at least in part necessary for S6K1 activity (ie. phosphorylation of S6) but S6K1 remains wholly dependent on mTOR kinase activity and thus sensitive to mTOR inhibition. A necessary-but-not-sufficient role for WNT4 in this pathway is consistent with similar characterization of WNT4 in the mammary gland [17, 36], and also suggests that other ER:WNT4 targets are critical mediators of proliferation and survival in ILC cells.

ER:WNT4 regulation of MCL1 is associated with metabolic dysregulation

Estrogen caused a decrease in levels of the BCL2-family protein MCL1, and this was reversed by WNT4 knockdown (**Figures 1-2**). ER regulation of MCL1 likely occurs post-transcriptionally, as qPCR determined that *MCL1* gene expression is not regulated by estrogen in ILC cells (**Supplemental Figure 4A**). Translational regulation of MCL1 has been previously linked to mTOR, with activation of mTOR signaling associated with increased MCL1 levels [37]. However, our data show that estrogen activates mTOR while suppressing MCL1, and targeting mTOR signaling does not similarly affect MCL1 levels (**Figure 3D**). Thus ER:WNT4 regulation of MCL1 is post-transcriptional but independent of mTOR signaling.

Given the canonical role of MCL1 as an anti-apoptotic BCL2-family protein [38], estrogen-driven reduction in MCL1 levels contrasts the important roles of ER:WNT4 in mediating cell survival [15]. However, reduction of MCL1 protein has been identified as critical to facilitate post-partum involution of uterine tissue [39]. Based on this, we hypothesized that estrogen-mediated repression of MCL1 may “prime” cells for apoptosis ([40]; ie. facilitate involution), but that anti-estrogens (inducing MCL1) would make ILC cells resistant to apoptosis. To test this, we treated ILC cells with BH3 mimetics alone or in combination with fulvestrant, or combined with MCL1-specific BH3 mimetic A-1210477. Though blocking MCL1 could moderately sensitize cells to other BH3 mimetics, fulvestrant caused no shifts in sensitivity to any tested combination of BH3 mimetics (**Supplemental Figure 4B**). This suggests ER:WNT4 regulation of MCL1 levels is not related to control of intrinsic apoptosis. MCL1 also plays a critical role in regulating mitochondrial dynamics [41–43], and based on this we hypothesized that

ER:WNT4 signaling may regulate mitochondrial function and metabolism in ILC cells. Consistent with this, siWNT4 causes both an increase in intracellular reactive oxygen species (ROS)(**Figure 3E**) and a decrease in total ATP content per cell (**Figure 3F**). These effects were not observed with siESR1, which parallels our prior observations that *WNT4* knockdown but not inhibition of ER induces cell death in ILC cells [15]. These data suggest that regulation of MCL1 is related to a critical role for WNT4 in mitochondrial metabolism.

WNT4 signaling is re-activated during anti-estrogen resistance in ILC cells

We previously reported that long-term estrogen deprived (LTED; mimicking AI-resistance) variants of ILC cell lines remain dependent on WNT4 [15], and hypothesized that WNT4-driven pathways identified in the parental cells would also be active in LTED models. LTED models 44:LTED/A and 134:LTED/E (derived from 44PE and MM134, respectively [15]) were analyzed by RPPA and compared to hormone-deprived parental cells to identify signaling adaptations during LTED. LTED cells were also transfected with siNT or siWNT4 as above to identify WNT4-driven signaling during LTED.

The majority of protein changes in LTED v parental comparisons were shared between models (**Figure 4A, Supplemental Figure 5A**). Of note, this included upregulation of FASN, confirming the transcriptional upregulation of *FASN* and lipid metabolism genes in these models that we recently reported (**Supplemental Figure 5B**) [44]. RPPA changes specific to 44:LTED/A (increased ER and OCT4) vs 134:LTED/E (decreased ER, increased phospho-NFκB) (**Supplemental Figure 5B**) also confirmed model-specific features of LTED that are linked to WNT4 upregulation as we reported previously [15]. Comparing protein changes in LTED models versus those caused by WNT4 knockdown (**Figure 4B-C**) identified 14 protein changes that are induced during LTED and mediated by WNT4 signaling (**Figure 4C-D**). WNT4-driven signaling in LTED included key ER:WNT4 targets described above, eg. S6 phosphorylation and MCL1 suppression, which were confirmed by immunoblotting (**Figure 4E**). These WNT4-driven signaling changes were also confirmed in our additional ILC:LTED cell lines (**Supplemental Figure 6**). Taken together, WNT4 regulation of downstream pathways, eg. cell cycle, mTOR signaling, and metabolism, remain active and critical to the LTED phenotype in ILC cells.

Atypical WNT4 signaling functions in diverse tumor types

To determine whether similar WNT4-driven signaling functions in tumor tissues (including other than ILC), we explored data from the Cancer Genome Atlas (TCGA). We examined tumors related to tissues that require WNT4 in development (eg. kidney, adrenal, lung, ovary, uterus [45–48]), and identified

tumors that over-expressed *WNT4* mRNA (**Figure 5A**). Comparing *WNT4* high versus other tumors, we looked for differences in protein signaling in RPPA data (reverse phase protein array). Renal clear cell carcinoma (RCC; total n=515, high *WNT4* n=89), lung adenocarcinoma (LuA; total n=533, high *WNT4* n=57), and serous ovarian cancer (OvCa; total n=307, high *WNT4* n=42) presented differences in protein signaling by RPPA in *WNT4* high tumors (**Supplemental Figure 7A**). Of note, other tumor types including ILC were limited by smaller sample sizes with RPPA data (eg. ILC, total n=160, high *WNT4* n=29). Comparing signaling changes in RCC, LuA, and OvCa (**Figure 5B**), OvCa was unique in having an upregulation of PI3K/mTOR pathway phospho-proteins in high *WNT4* tumors (**Supplemental Figure 7A-B**). Shared signaling changes were limited; differentially regulated proteins in all 3 tumors types (n=10) were not similarly induced/repressed in all three tumors, with the exception of high *WNT4* being associated with decreased ER levels (**Supplemental Figure 7C**). Changes in total β-catenin in high *WNT4* tumors was seen in LuA and RCC, but not OvCa (**Supplemental Figure 7D**), suggesting that WNT4 in OvCa may activate non-canonical signaling that converges on mTOR as in ILC. Similar to our observations in ILC cell lines, high *WNT4* in OvCa was associated with increased phosphorylation of 4EBP1, p70-S6K, and S6 (**Figure 5C**). Further, high *WNT4* expression in OvCa was associated with shorter overall survival (median OS, 28.5mo v 45.0mo; **Figure 5D**). Though RPPA data for ILC tumors were too limited to identify associations with active mTOR signaling, high *WNT4* was associated with decreased PTEN protein levels, consistent with activated downstream signaling (**Supplemental Figure 7E**). Additionally, high *WNT4* was associated with decreased phospho-Akt-S473, paralleling low phospho-Akt levels in our cell line data. These data suggest that non-canonical WNT4 signaling via the mTOR pathway may be critical in multiple tumor types, including ILC and OvCa.

Discussion

Clinical and laboratory data support that ILC represents a unique context for estrogen receptor signaling, which may be mediated in part by ER induced *WNT4* expression. The Wnt ligand WNT4 plays a critical role in the normal development of the mammary gland, and plays a similar role in endocrine response and resistance in ILC [15]. However, given the myriad tissue-specific pathways targeted by WNT4, and dysfunctional β-catenin-dependent signaling in ILC [4, 15, 16], it is unclear how WNT4 mediates proliferation and survival in ILC cells. To address this, we used RPPA analyses to profile ER-driven signaling in ILC cells, identify ER-driven signaling that requires WNT4 (ie. ER:WNT4 signaling), and assess the activity of these pathways in anti-estrogen resistance. Our studies identified that in ILC cells, ER:WNT4 signaling mediates downstream activity of mTOR signaling via p70-S6K, as WNT4 knockdown suppresses S6 phosphorylation. We also identified that ER:WNT4 signaling led to a suppression of total MCL1 levels, which was not associated with differential sensitivity to pro-apoptotic dugs, but instead with metabolic dysfunction upon WNT4 knockdown. Parallel signaling mediated by WNT4 was identified in anti-estrogen-resistant models of ILC, and related signaling pathways were also linked to *WNT4* overexpression in serous ovarian cancer. These data provide new insight in to a poorly understood Wnt signaling pathway, and identify potential downstream signaling pathways that may be targetable to inhibit cell proliferation and survival mediated by WNT4.

Though WNT4 itself has not been mechanistically linked directly to mTOR signaling previously, β-catenin-independent Wnt signaling was shown by Inoki et al to regulate mTOR activity via GSK3, independent of Akt phosphorylation [29]. Since we did not detect E2-induced AKT phosphorylation but GSK3 phosphorylation was strongly E2-induced in ILC cells (**Figure 1**), this may represent the pathway linking WNT4 to mTOR. GSK3 phosphorylation was also among the most strongly increased signaling events in high *WNT4*-expressing OvCa (**Supplemental Figure 7B**). However, GSK3 phosphorylation did not appear to be affected by WNT4 knockdown in ILC cells by RPPA (**Figure 2**, **Supplemental Figure 2**). Further, whereas Inoki et al also showed that Wnt signaling modulated p70-S6K phosphorylation (T389), we observed that while estrogen did increase phosphorylation at this residue, WNT4 knockdown had no effect on p70-S6K-T389 phosphorylation (**Figure 3**). Direct inhibition of p70-S6K using PF-4708671 also does not block T389 phosphorylation [35], but WNT4 may regulate p70-S6K phosphorylation at an alternative site, or regulate p70-S6K cellular localization [49].

Three independent large-scale genomic analyses of ILC cohorts have described activation of PI3K/Akt signaling in ILC as a major feature of this tumor type, including increased activity of this pathway versus matched IDC tumors [4–6]. Pathway activation is linked to reduced PTEN protein levels in ILC,

increased phospho-Akt, and increased phospho-p70-S6K [4]. These observations parallel our data identifying that ER drives downstream mTOR signaling in ILC cells. In contrast, we observed that ILC cells have low levels of total and phospho-Akt versus MCF-7 cells. As described above, WNT4 in ILC may represent an alternative pathway for the activation of mTOR signaling, potentially in concert with estrogen regulation of *WNT4* and low PTEN, as high *WNT4*-expressing ILC also had decreased phospho-Akt (**Supplemental Figure 7E**). A recent study by Teo et al linked Akt activation to loss of E-cadherin (the hallmark feature of ILC [4]), but these studies identified this link using ER-negative ILC models (murine p53/CDH1-null lines and IPH-926)[50]. These observations suggest that even within ILC, subsets with distinct modes of PI3K/Akt/mTOR signaling exist. Supporting this, among Luminal A ILC, TCGA RPPA identified differential levels and phosphorylation of PI3K/Akt/mTOR pathway proteins across mRNA subtypes (e.g. low p70S6K and Raptor in Reactive; high phospho-PRAS40 and phospho-mTOR in immune; Proliferative lacked distinct differences in this pathway). Another important context for PI3K-pathway signaling in ILC is likely the tumor microenvironment and metastasis. Tasdemir et al recently reported that in ultra-low attachment conditions (ie. requiring anchorage-independence), ILC cell lines uniquely sustained PI3K-pathway activation versus IDC cell lines [51]. Further mechanistic studies are needed to link biomarkers with PI3K/Akt/mTOR signaling activity to identify personalized targets for therapy.

The putative link between ER:WNT signaling and MCL1/mitochondrial function suggests that WNT4 is critical for cellular metabolism in ILC. We observed that WNT4 knockdown leads to an accumulation of cellular ROS that parallels impaired ATP production (**Figure 3**), and both of these phenotypes precede the induction of cell death (~4d post-siWNT4 transfection, [15]). This suggests that WNT4-mediated control of metabolism and/or mitochondrial function are critical to ILC cell survival. Wnt signaling (both β-catenin-dependent and -independent signaling) has been previously linked to these processes [52–54], but roles for WNT4 in mitochondrial function have not previously described. However, one recent study demonstrated that Wnt4 overexpression could rescue a defect in mitochondrial function and dynamics caused by deletion of PTEN-inducible kinase 1 (PINK1) in Drosophila [55]. Though the mechanism of rescue is unclear, Wnt4 over-expression rescued flight defects in the PINK1 knockout flies, increasing ATP production and restoring mitochondria membrane potential in flight muscles. Future studies will further examine whether WNT4 plays a similar role in cancer cells. Metabolic defects caused by WNT4 knockdown may also be caused by suppressing WNT4 signaling using anti-estrogens or mTOR pathway inhibitors. Targeting therapy-induced metabolic vulnerability may be a powerful combination treatment approach for WNT4-driven cancers.

The similar signaling pathways associated with WNT4 in ILC and OvCa may parallel the critical role of WNT4 in the tissues of origin, as well as related tumor biology. In addition to being required for mammary gland development, WNT4 is required for the development of the ovary and Mullerian tissues [45, 56], female sex differentiation [56, 57], and fertility [46, 58]. Accordingly, WNT4 dysfunction is linked to a range of endocrine and gynecologic pathologies, including endometriosis [59], uterine fibroids [60], and ovarian cancer [61]. For ovarian cancer that originates from fallopian tube epithelium (FTE), transformed FTE cells must migrate to and invade the ovary to establish a tumor. WNT4 is required for cell migration and ovary invasion in murine PTEN-null models of FTE-derived ovarian cancer [62], suggesting that WNT4 is critical in early ovarian tumorigenesis. Perhaps consistent with this role of WNT4 in migration/invasion, both OvCa and ILC metastasize to the abdomen/peritoneal cavity, ILC being unique among breast cancers in this regard [63, 64]. Defining WNT4 signaling in these tumors may provide new insight in to targeting metastatic OvCa and ILC.

WNT4 signaling is a key mediator of endocrine response and resistance in ILC, but in particular given the dysfunction of β-catenin-dependent signaling in ILC, WNT4 signaling is poorly defined. In this study, we used RPPA analyses to identify mTOR signaling and MCL1/mitochondrial function as two key downstream effectors of WNT4 in ILC. Parallel pathways associated with WNT4 were also identified in serous ovarian cancer, suggesting that WNT4 signaling is important in multiple tumor types. Future studies will determine how WNT4 is mechanistically linked to these targets, including identification of the WNT4 receptor in ILC. Furthering our understanding of WNT4 signaling will improve opportunities for precision treatment approaches by targeting WNT4 signaling for patients with ILC or OvCa, and support the development of strategies to overcome anti-estrogen resistance for patients with ILC.

Acknowledgements

We thank Jian Chen (UPMC Hillman Cancer Center) for technical support.

References

1. Sikora MJ, Jabobsen BM, O'Connor DP, Riggins RB, Stires H, Oesterreich S. ILC-CORE (Collaboration, Openness, REproducibility). Open Sci Framew. 2017;19 Sept.(http://doi.org/10.17605/OSF.IO/7X8NG).
2. Sikora MJ, Jankowitz RC, Dabbs DJ, Oesterreich S. Invasive lobular carcinoma of the breast: patient response to systemic endocrine therapy and hormone response in model systems. Steroids. Elsevier Inc.; 2013 Jun;78(6):568–575. PMID: 23178159
3. Dossus L, Benusiglio PR. Lobular breast cancer: incidence and genetic and non-genetic risk factors. Breast Cancer Res. BioMed Central; 2015;17(1):37. PMID: 25848941
4. Ciriello G, Gatza ML, Beck AH, Wilkerson MD, Rhie SK, Pastore A, et al. Comprehensive Molecular Portraits of Invasive Lobular Breast Cancer. Cell. 2015 Oct 8;163(2):506–519. PMID: 26451490
5. Desmedt C, Zoppoli G, Gundem G, Pruneri G, Larsimont D, Fornili M, et al. Genomic Characterization of Primary Invasive Lobular Breast Cancer. J Clin Oncol. 2016 Jun 1;34(16):1872–81. PMID: 26926684
6. Michaut M, Chin S-F, Majewski I, Severson TM, Bismeijer T, de Koning L, et al. Integration of genomic, transcriptomic and proteomic data identifies two biologically distinct subtypes of invasive lobular breast cancer. Sci Rep. 2016 Jan;6:18517. PMID: 26729235
7. Metzger Filho O, Giobbie-Hurder A, Mallon E, Gusterson B, Viale G, Winer EP, et al. Relative Effectiveness of Letrozole Compared With Tamoxifen for Patients With Lobular Carcinoma in the BIG 1-98 Trial. J Clin Oncol. 2015 Sep 1;33(25):2772–9. PMID: 26215945
8. Knauer M, Gruber C, Dietze O, Greil R, Stöger H, Rudas M, et al. Abstract S2-06: Survival advantage of anastrozol compared to tamoxifen for lobular breast cancer in the ABCSG-8 study. Cancer Res. 2015 Apr 30;75(9 Supplement):S2-06-S2-06.
9. Colleoni M, Rotmensz N, Maisonneuve P, Mastropasqua MG, Luini A, Veronesi P, et al. Outcome of special types of luminal breast cancer. Ann Oncol Off J Eur Soc Med Oncol. 2012 Jun;23(6):1428–36. PMID: 22039080
10. Pestalozzi BC, Zahrieh D, Mallon E, Gusterson BA, Price KN, Gelber RD, et al. Distinct clinical and prognostic features of infiltrating lobular carcinoma of the breast: combined results of 15 International Breast Cancer Study Group clinical trials. J Clin Oncol. 2008 Jun 20;26(18):3006–14. PMID: 18458044
11. Rakha EA, El-Sayed ME, Powe DG, Green AR, Habashy H, Grainge MJ, et al. Invasive lobular carcinoma of the breast: response to hormonal therapy and outcomes. Eur J Cancer. 2008 Jan;44(1):73–83. PMID: 18035533
12. Chen Z, Yang J, Li S, Lv M, Shen Y, Wang B, et al. Invasive lobular carcinoma of the breast: A special histological type compared with invasive ductal carcinoma. PLoS One. 2017;12(9):e0182397. PMID: 28863134
13. Sikora MJ, Cooper KL, Bahreini A, Luthra S, Wang G, Chandran UR, et al. Invasive lobular carcinoma cell lines are characterized by unique estrogen-mediated gene expression patterns and altered tamoxifen response. Cancer Res. 2014 Mar 1;74(5):1463–74. PMID: 24425047
14. Tasdemir N, Bossart EA, Li Z, Zhu L, Sikora MJ, Levine KM, et al. Comprehensive Phenotypic Characterization of Human Invasive Lobular Carcinoma Cell Lines in 2D and 3D Cultures. Cancer Res. 2018 Nov 1;78(21):6209–6222. PMID: 30228172
15. Sikora MJ, Jacobsen BM, Levine K, Chen J, Davidson NE, Lee A V, et al. WNT4 mediates estrogen receptor signaling and endocrine resistance in invasive lobular carcinoma cell lines. Breast Cancer Res. Breast Cancer Research; 2016 Sep 20;18(1):92. PMID: 27650553

16. Rao DM, Bordeaux EK, Yamamoto TM, Bitler BG, Sikora MJ. WNT4 and WNT3A activate cell autonomous Wnt signaling independent of secretion. bioRxiv. Cold Spring Harbor Laboratory; 2018 May 30;333906 [Pre-print].
17. Brisken C, Heineman A, Chavarria T, Elenbaas B, Tan J, Dey SK, et al. Essential function of Wnt-4 in mammary gland development downstream of progesterone signaling. Genes Dev. 2000 Mar 15;14(6):650–4. PMID: 10733525
18. Rajaram RD, Buric D, Caikovski M, Ayyanan A, Rougemont J, Shan J, et al. Progesterone and Wnt4 control mammary stem cells via myoepithelial crosstalk. EMBO J. 2015 Mar 4;34(5):641–52. PMID: 25603931
19. Joshi PA, Jackson HW, Beristain AG, Di Grappa MA, Mote PA, Clarke CL, et al. Progesterone induces adult mammary stem cell expansion. Nature. 2010 Jun;465(7299):803–807. PMID: 20445538
20. Meier-Abt F, Milani E, Roloff T, Brinkhaus H, Duss S, Meyer DS, et al. Parity induces differentiation and reduces Wnt/Notch signaling ratio and proliferation potential of basal stem/progenitor cells isolated from mouse mammary epithelium. Breast Cancer Res. 2013 Apr 29;15(2):R36. PMID: 23621987
21. Sikora MJ, Johnson MD, Lee A V, Oesterreich S. Endocrine Response Phenotypes Are Altered by Charcoal-Stripped Serum Variability. Endocrinology. 2016 Oct 26;157(10):3760–3766. PMID: 27459541
22. MD Anderson Cancer Center Functional Proteomics Core Facility. PREPARATION OF CELL LYSATE FOR REVERSE PHASE PROTEIN ARRAY (6 -WELL FORMAT) [Inte https://www.mdanderson.org/documents/core-facilities/Functional Proteomics RPPA Core Facility/RPPA_6 Well Plate Lysate Prep.pdf. 2016.
23. Bossart EA, Tasdemir N, Sikora MJ, Bahreini A, Levine KM, Chen J, et al. SNAIL is induced by tamoxifen and leads to growth inhibition in invasive lobular breast carcinoma. Breast Cancer Res Treat. 2019 Jun;175(2):327–337. PMID: 30798422
24. Cook AJL, Gurard-Levin ZA, Vassias I, Almouzni G. A specific function for the histone chaperone NASP to fine-tune a reservoir of soluble H3-H4 in the histone supply chain. Mol Cell. 2011 Dec 23;44(6):918–27. PMID: 22195965
25. Alvarez F, Muñoz F, Schilcher P, Imhof A, Almouzni G, Loyola A. Sequential establishment of marks on soluble histones H3 and H4. J Biol Chem. American Society for Biochemistry and Molecular Biology; 2011 May 20;286(20):17714–21. PMID: 21454524
26. Zentner GE, Henikoff S. Regulation of nucleosome dynamics by histone modifications. Nat Struct Mol Biol. Nature Publishing Group; 2013 Mar 5;20(3):259–66. PMID: 23463310
27. Hammond CM, Strømme CB, Huang H, Patel DJ, Groth A. Histone chaperone networks shaping chromatin function. Nat Rev Mol Cell Biol. Nature Research; 2017 Mar 5;18(3):141–158. PMID: 28053344
28. Ahmad S, Singh N, Glazer RI. Role of AKT1 in 17beta-estradiol- and insulin-like growth factor I (IGF-I)-dependent proliferation and prevention of apoptosis in MCF-7 breast carcinoma cells. Biochem Pharmacol. 1999 Aug 1;58(3):425–30. PMID: 10424760
29. Inoki K, Ouyang H, Zhu T, Lindvall C, Wang Y, Zhang X, et al. TSC2 integrates Wnt and energy signals via a coordinated phosphorylation by AMPK and GSK3 to regulate cell growth. Cell. 2006 Sep 8;126(5):955–68. PMID: 16959574
30. Yang W, Schwartz GN, Marotti JD, Chen V, Traphagen NA, Gui J, et al. Estrogen receptor alpha drives mTORC1 inhibitor-induced feedback activation of PI3K/AKT in ER+ breast cancer. Oncotarget. 2018 Feb 6;9(10):8810–8822. PMID: 29507656
31. Millour J, Constantinidou D, Stavropoulou a V, Wilson MSC, Myatt SS, Kwok JM-M, et al. FOXM1 is a transcriptional target of ERalpha and has a critical role in breast cancer endocrine sensitivity and resistance. Oncogene. Nature Publishing Group; 2010 May 20;29(20):2983–95. PMID: 20208560
32. Sanders DA, Ross-Innes CS, Beraldi D, Carroll JS, Balasubramanian S. Genome-wide mapping

of FOXM1 binding reveals co binding with estrogen receptor alpha in breast cancer cells. Genome Biol. 2013 Jan 24;14(1):R6. PMID: 23347430
33. Bergamaschi A, Madak-Erdogan Z, Kim YJ, Choi Y-L, Lu H, Katzenellenbogen BS. The forkhead transcription factor FOXM1 promotes endocrine resistance and invasiveness in estrogen receptor-positive breast cancer by expansion of stem-like cancer cells. Breast Cancer Res. 2014;16(5):436. PMID: 25213081
34. Gormally M V, Dexheimer TS, Marsico G, Sanders D a, Lowe C, Matak-Vinković D, et al. Suppression of the FOXM1 transcriptional programme via novel small molecule inhibition. Nat Commun. 2014;5:5165. PMID: 25387393
35. Pearce LR, Alton GR, Richter DT, Kath JC, Lingardo L, Chapman J, et al. Characterization of PF-4708671, a novel and highly specific inhibitor of p70 ribosomal S6 kinase (S6K1). Biochem J. 2010 Oct 15;431(2):245–55. PMID: 20704563
36. Kim YC, Clark RJ, Pelegri F, Alexander CM. Wnt4 is not sufficient to induce lobuloalveolar mammary development. BMC Dev Biol. 2009 Oct 30;9(1):55. PMID: 19878558
37. Anderson GR, Wardell SE, Cakir M, Crawford L, Leeds JC, Nussbaum DP, et al. PIK3CA mutations enable targeting of a breast tumor dependency through mTOR-mediated MCL-1 translation. Sci Transl Med. 2016 Dec 14;8(369):369ra175. PMID: 27974663
38. Opferman JT, Iwasaki H, Ong CC, Suh H, Mizuno S, Akashi K, et al. Obligate role of anti-apoptotic MCL-1 in the survival of hematopoietic stem cells. Science. 2005 Feb 18;307(5712):1101–4. PMID: 15718471
39. Kyathanahalli C, Marks J, Nye K, Lao B, Albrecht ED, Aberdeen GW, et al. Cross-species withdrawal of MCL1 facilitates postpartum uterine involution in both the mouse and baboon. Endocrinology. 2013 Dec 1;154(12):4873–84. PMID: 24140717
40. Potter DS, Letai A. To Prime, or Not to Prime: That Is the Question. Cold Spring Harb Symp Quant Biol. 2016;81:131–140. PMID: 27811212
41. Morciano G, Pedriali G, Sbano L, Iannitti T, Giorgi C, Pinton P. Intersection of mitochondrial fission and fusion machinery with apoptotic pathways: Role of Mcl-1. Biol cell. 2016 Oct;108(10):279–293. PMID: 27234233
42. Perciavalle RM, Opferman JT. Delving deeper: MCL-1's contributions to normal and cancer biology. Trends Cell Biol. Elsevier Ltd; 2013;23(1):22–29. PMID: 23026029
43. Morciano G, Giorgi C, Balestra D, Marchi S, Perrone D, Pinotti M, et al. Mcl-1 involvement in mitochondrial dynamics is associated with apoptotic cell death. Mol Biol Cell. 2016 Jan 1;27(1):20–34. PMID: 26538029
44. Du T, Sikora MJ, Levine KM, Tasdemir N, Riggins RB, Wendell SG, et al. Key regulators of lipid metabolism drive endocrine resistance in invasive lobular breast cancer. Breast Cancer Res. 2018 Sep 4;20(1):106. PMID: 30180878
45. Vainio S, Heikkilä M, Kispert A, Chin N, McMahon AP. Female development in mammals is regulated by Wnt-4 signalling. Nature. 1999 Feb 4;397(6718):405–9. PMID: 9989404
46. Boyer A, Lapointe E, Zheng X, Cowan RG, Li H, Quirk SM, et al. WNT4 is required for normal ovarian follicle development and female fertility. FASEB J. 2010 Aug;24(8):3010–25. PMID: 20371632
47. Biason-Lauber A, De Filippo G, Konrad D, Scarano G, Nazzaro A, Schoenle EJ. WNT4 deficiency--a clinical phenotype distinct from the classic Mayer-Rokitansky-Kuster-Hauser syndrome: a case report. Hum Reprod. 2007 Jan;22(1):224–9. PMID: 16959810
48. Caprioli A, Villasenor A, Wylie LA, Braitsch C, Marty-Santos L, Barry D, et al. Wnt4 is essential to normal mammalian lung development. Dev Biol. 2015 Oct 15;406(2):222–34. PMID: 26321050
49. Rosner M, Hengstschläger M. Nucleocytoplasmic localization of p70 S6K1, but not of its isoforms p85 and p31, is regulated by TSC2/mTOR. Oncogene. 2011 Nov 3;30(44):4509–22. PMID: 21602892
50. Teo K, Gómez-Cuadrado L, Tenhagen M, Byron A, Rätze M, van Amersfoort M, et al. E-cadherin loss induces targetable autocrine activation of growth factor signalling in lobular breast cancer.

Sci Rep. 2018 Oct;8(1):15454. PMID: 30337563
51. Tasdemir N, Ding K, Levine KM, Du T, Bossart EA, Adrian V. Proteomic and Transcriptomic Profiling Identifies Mediators of Anchorage- Independent Growth and Roles of Inhibitor of Differentiation Proteins in Invasive Lobular Breast Cancer. bioRxiv. 2019;543132 [Pre-print].
52. Bernkopf DB, Jalal K, Brückner M, Knaup KX, Gentzel M, Schambony A, et al. Pgam5 released from damaged mitochondria induces mitochondrial biogenesis via Wnt signaling. J Cell Biol. 2018;217(4):1383–1394. PMID: 29438981
53. Godoy JA, Arrázola MS, Ordenes D, Silva-Alvarez C, Braidy N, Inestrosa NC. Wnt-5a ligand modulates mitochondrial fission-fusion in rat hippocampal neurons. J Biol Chem. 2014 Dec;289(52):36179–93. PMID: 25336659
54. Pate KT, Stringari C, Sprowl-Tanio S, Wang K, TeSlaa T, Hoverter NP, et al. Wnt signaling directs a metabolic program of glycolysis and angiogenesis in colon cancer. EMBO J. 2014 Jul;33(13):1454–73. PMID: 24825347
55. Wu W, Han Y, Fan X, Li Q, Sun L. Protective mechanism of Wnt4 gene on Parkinson's disease (PD) transgenic Drosophila. Int J Neurosci. 2019 Jul;129(7):703–714. PMID: 30526176
56. Philibert P, Biason-Lauber A, Rouzier R, Pienkowski C, Paris F, Konrad D, et al. Identification and functional analysis of a new WNT4 gene mutation among 28 adolescent girls with primary amenorrhea and müllerian duct abnormalities: a French collaborative study. J Clin Endocrinol Metab. 2008 Mar;93(3):895–900. PMID: 18182450
57. Biason-Lauber A. WNT4, RSPO1, and FOXL2 in sex development. Semin Reprod Med. 2012 Oct;30(5):387–95. PMID: 23044875
58. Zhang G, Feenstra B, Bacelis J, Liu X, Muglia LJLMLJ, Juodakis J, et al. Genetic Associations with Gestational Duration and Spontaneous Preterm Birth. N Engl J Med. 2017 Sep 21;377(12):1156–1167. PMID: 28877031
59. Nyholt DR, Low S-K, Anderson CA, Painter JN, Uno S, Morris AP, et al. Genome-wide association meta-analysis identifies new endometriosis risk loci. Nat Genet. Nature Publishing Group; 2012 Dec;44(12):1355–9. PMID: 23104006
60. Välimäki N, Kuisma H, Pasanen A, Heikinheimo O, Sjöberg J, Bützow R, et al. Genetic predisposition to uterine leiomyoma is determined by loci for genitourinary development and genome stability. Elife. 2018 Sep 18;7. PMID: 30226466
61. Kuchenbaecker KB, Ramus SJ, Tyrer J, Lee A, Shen HC, Beesley J, et al. Identification of six new susceptibility loci for invasive epithelial ovarian cancer. Nat Genet. 2015 Feb;47(2):164–71. PMID: 25581431
62. Russo A, Czarnecki AA, Dean M, Modi DA, Lantvit DD, Hardy L, et al. PTEN loss in the fallopian tube induces hyperplasia and ovarian tumor formation. Oncogene. 2018 Apr 12;37(15):1976–1990. PMID: 29367766
63. Arpino G, Bardou VJ, Clark GM, Elledge RM. Infiltrating lobular carcinoma of the breast: tumor characteristics and clinical outcome. Breast Cancer Res. 2004 Jan;6(3):R149-56. PMID: 15084238
64. Mathew A, Rajagopal PS, Villgran V, Sandhu GS, Jankowitz RC, Jacob M, et al. Distinct Pattern of Metastases in Patients with Invasive Lobular Carcinoma of the Breast. Geburtshilfe Frauenheilkd. 2017 Jun;77(6):660–666. PMID: 28757653

FIGURE 1

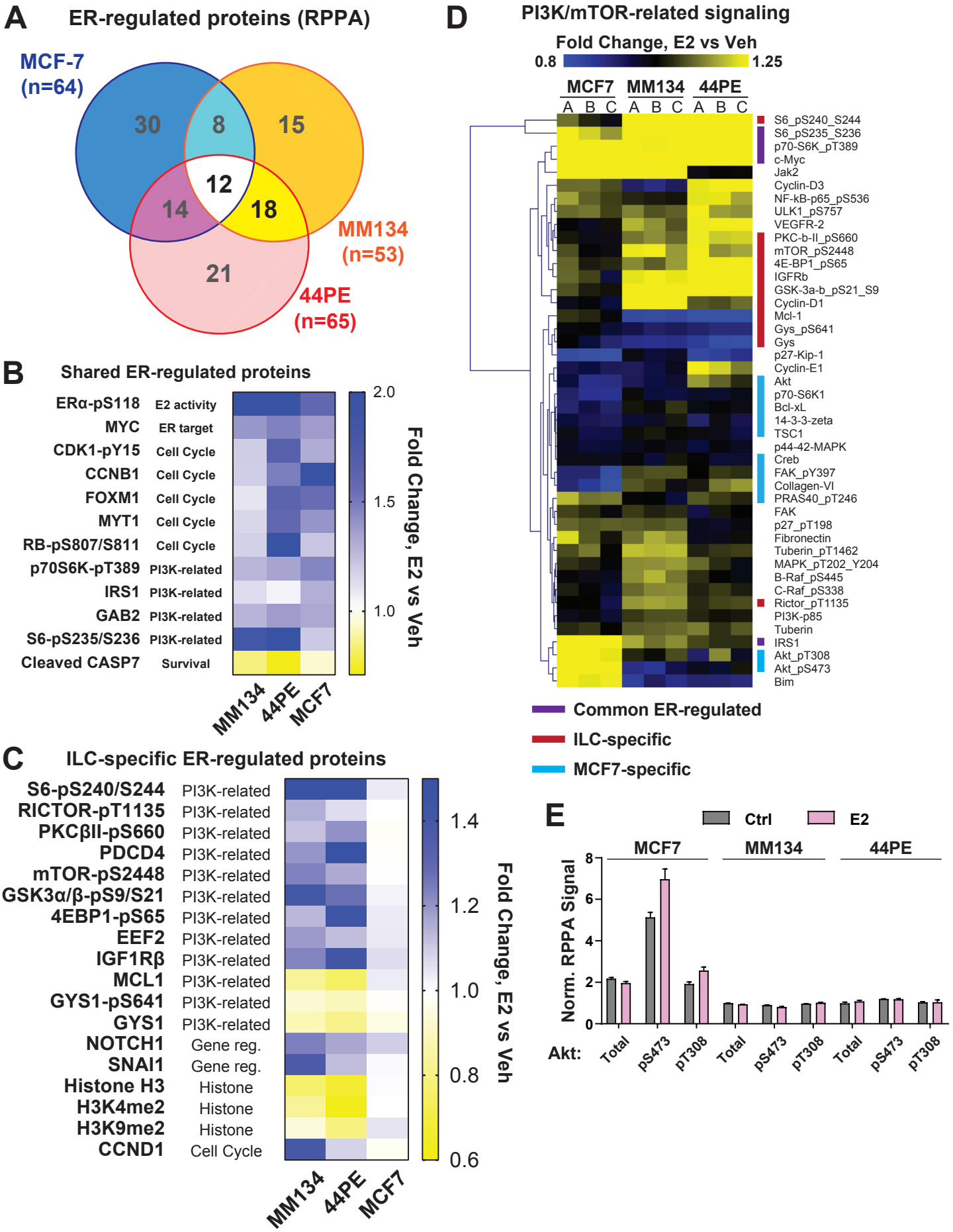
A
ER-regulated proteins (RPPA)
MCF-7
(n=64)
MM134
(n=53)
44PE
(n=65)
30
8
15
12
14
18
21
B
Shared ER-regulated proteins
ERα-pS118 E2 activity
MYC ER target
CDK1-pY15 Cell Cycle
CCNB1 Cell Cycle
FOXM1 Cell Cycle
MYT1 Cell Cycle
RB-pS807/S811 Cell Cycle
p70S6K-pT389 PI3K-related
IRS1 PI3K-related
GAB2 PI3K-related
S6-pS235/S236 PI3K-related
Cleaved CASP7 Survival
MM134
44PE
MCF7
2.0
1.5
1.0
Fold Change, E2 vs Veh
C
ILC-specific ER-regulated proteins
S6-pS240/S244 PI3K-related
RICTOR-pT1135 PI3K-related
PKCβII-pS660 PI3K-related
PDCD4 PI3K-related
mTOR-pS2448 PI3K-related
GSK3α/β-pS9/S21 PI3K-related
4EBP1-pS65 PI3K-related
EEF2 PI3K-related
IGF1Rβ PI3K-related
MCL1 PI3K-related
GYS1-pS641 PI3K-related
GYS1 PI3K-related
NOTCH1 Gene reg.
SNAI1 Gene reg.
Histone H3 Histone
H3K4me2 Histone
H3K9me2 Histone
CCND1 Cell Cycle
MM134
44PE
MCF7
1.4
1.2
1.0
0.8
0.6
Fold Change, E2 vs Veh
D
PI3K/mTOR-related signaling
Fold Change, E2 vs Veh
0.8
1.25
MCF7 MM134 44PE
A B C A B C A B C
S6_pS240_S244
S6_pS235_S236
p70-S6K_pT389
c-Myc
Jak2
Cyclin-D3
NF-kB-p65_pS536
ULK1_pS757
VEGFR-2
PKC-b-II_pS660
mTOR_pS2448
4E-BP1_pS65
IGFRb
GSK-3a-b_pS21_S9
Cyclin-D1
Mcl-1
Gys_pS641
Gys
p27-Kip-1
Cyclin-E1
Akt
p70-S6K1
Bcl-xL
14-3-3-zeta
TSC1
p44-42-MAPK
Creb
FAK_pY397
Collagen-VI
PRAS40_pT246
FAK
p27_pT198
Fibronectin
Tuberin_pT1462
MAPK_pT202_Y204
B-Raf_pS445
C-Raf_pS338
Rictor_pT1135
PI3K-p85
Tuberin
IRS1
Akt_pT308
Akt_pS473
Bim
Common ER-regulated
ILC-specific
MCF7-specific
E
Ctrl
E2
MCF7
MM134
44PE
Norm. RPPA Signal
8
6
4
2
0
Akt:
Total
pS473
pT308
Total
pS473
pT308
Total
pS473
pT308

Figure 1. Estrogen regulates distinct protein targets in ILC cells versus MCF-7 cells. A) Cells were hormone-deprived prior to treatment with 100pM E2 for 24hrs (biological triplicate; see Materials and Methods). RPPA protein signaling changes for 100pM E2 vs Veh shown ($q<0.05$ for MM134, 44PE; $p<0.05$ for MCF-7). **B-C)** Heatmap for E2 vs Veh fold change (mean of triplicate samples). **D)** PI3K pathway proteins were identified using KEGG pathways for PI3K/Akt/mTOR signaling. A/B/C represent biological replicate samples. **E)** Normalized Linear RPPA signal for total Akt or phospho-Akt (antibodies recognize AKT1/AKT2/AKT3).

FIGURE 2

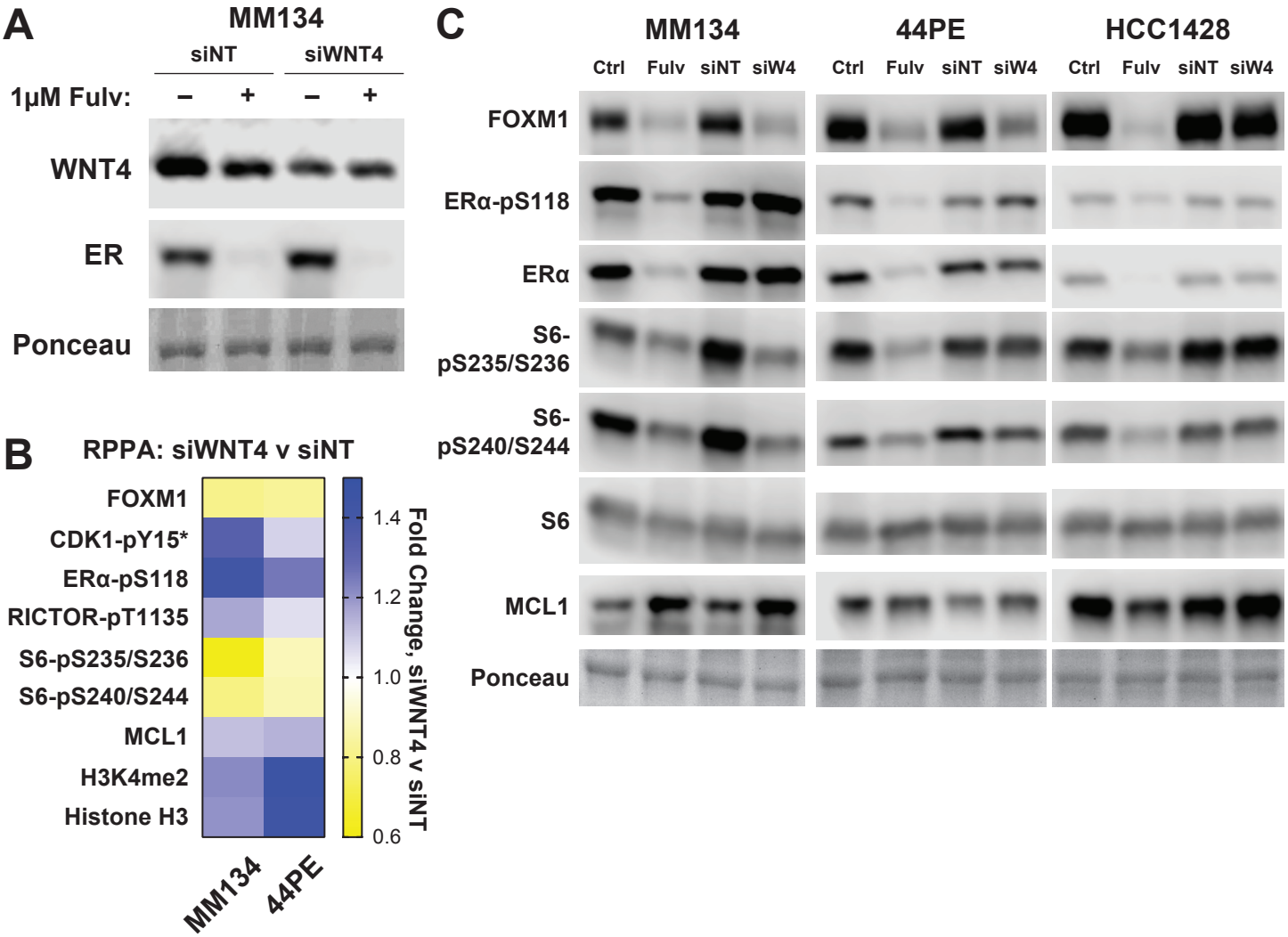
A
MM134
siNT
siWNT4
1μM Fulv:
–
+
–
+
WNT4
ER
Ponceau
B
RPPA: siWNT4 v siNT
FOXM1
CDK1-pY15*
ERα-pS118
RICTOR-pT1135
S6-pS235/S236
S6-pS240/S244
MCL1
H3K4me2
Histone H3
MM134
44PE
1.4
1.2
1.0
0.8
0.6
Fold Change, siWNT4 v siNT
C
MM134
44PE
HCC1428
Ctrl
Fulv
siNT
siW4
FOXM1
ERα-pS118
ERα
S6-pS235/S236
S6-pS240/S244
S6
MCL1
Ponceau

Figure 2. WNT4 is required for key components of ER signaling. A) MM134 cells in full serum were reverse transfected with the indicated siRNA. 24hrs later, cells were treated with Fulv, and lysates were harvested an additional 24hrs later. **B)** Cells were hormone-deprived prior to siRNA reverse transfection and subsequent treatment with 100pM E2 for 24hrs (biological triplicate; see Materials and Methods). RPPA protein signaling changes for siWNT4+E2 versus siNT+E2 shown ($p<0.05$) which overlapped with E2-driven signaling identified in Figure 1. *, siWNT4 effect is a false positive due to siNT-mediated suppression of signal versus E2/mock transfected (from Figure 1). **C)** Cells were transfected and treated as in (A).

FIGURE 3

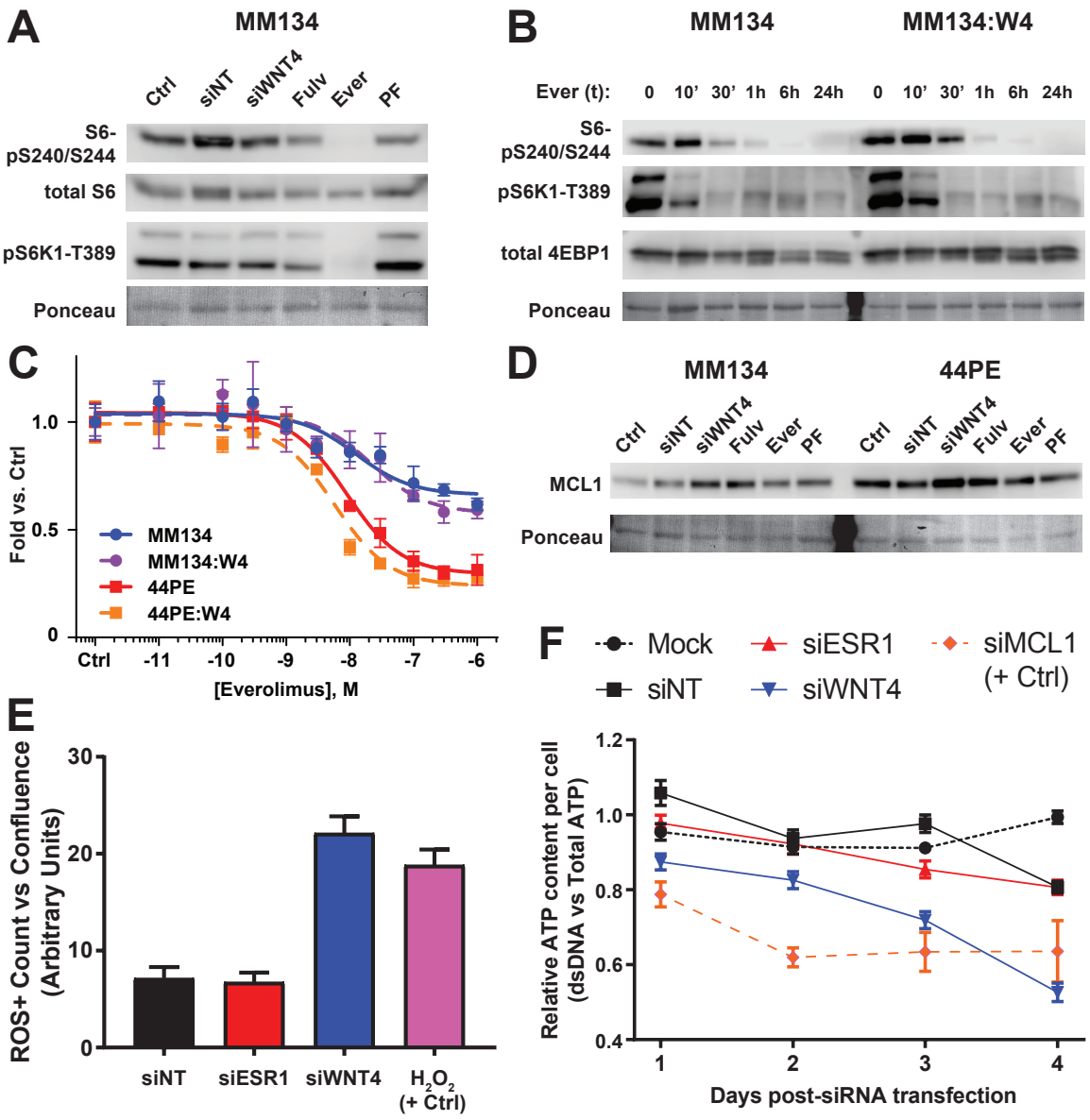
A
MM134
Ctrl
siNT
siWNT4
Fulv
Ever
PF
S6-pS240/S244
total S6
pS6K1-T389
Ponceau
B
MM134
MM134:W4
Ever (t):
0 10' 30' 1h 6h 24h 0 10' 30' 1h 6h 24h
S6-pS240/S244
pS6K1-T389
total 4EBP1
Ponceau
C
Fold vs. Ctrl
1.0
0.5
0
MM134
MM134:W4
44PE
44PE:W4
Ctrl -11 -10 -9 -8 -7 -6
[Everolimus], M
D
MM134
44PE
Ctrl siNT siWNT4 Fulv Ever PF Ctrl siNT siWNT4 Fulv Ever PF
MCL1
Ponceau
E
ROS+ Count vs Confluence (Arbitrary Units)
30
20
10
0
siNT
siESR1
siWNT4
H2O2 (+ Ctrl)
F
Mock
siNT
siESR1
siWNT4
siMCL1 (+ Ctrl)
Relative ATP content per cell (dsDNA vs Total ATP)
1.2
1.0
0.8
0.6
0.4
1 2 3 4
Days post-siRNA transfection

Figure 3. WNT4 independently controls S6 phosphorylation, and mitochondrial function associated with MCL1 levels. A) MM134 cells in full serum were either reverse transfected with the indicated siRNA for 48hrs, or treated with 100nM Fulvestrant, 100nM Everolimus, or 10μM PF-04708671 for 24hrs. **B)** Cells in full serum were treated with 100nM Everolimus for the indicated time. Total 4EBP1 shows a downward shift in mobility consistent with decreased phosphorylation after everolimus treatment. **C)** Cells were treated with increasing concentrations of Everolimus as indicated in biological replicates of 6 for 6d; total cell number was assessed by dsDNA quantification. Points represent mean±SD. **D)** Cells were transfected and treated as in (A).**E)** Total ROS was measured in MM134 cells 48hr post-transfection; 1mM H_2O_2 treatment for 30m served as a positive control. Bars represent mean of 5 biological replicates ±SD. **F)** MM134 cells were transfected with the indicated siRNA (reduced siRNA concentration of 2.5nM used for MCL1), and samples were collected for dsDNA and total ATP quantification at the indicated timepoint. Points indicate mean of 6 biological replicates ±SD.

FIGURE 4

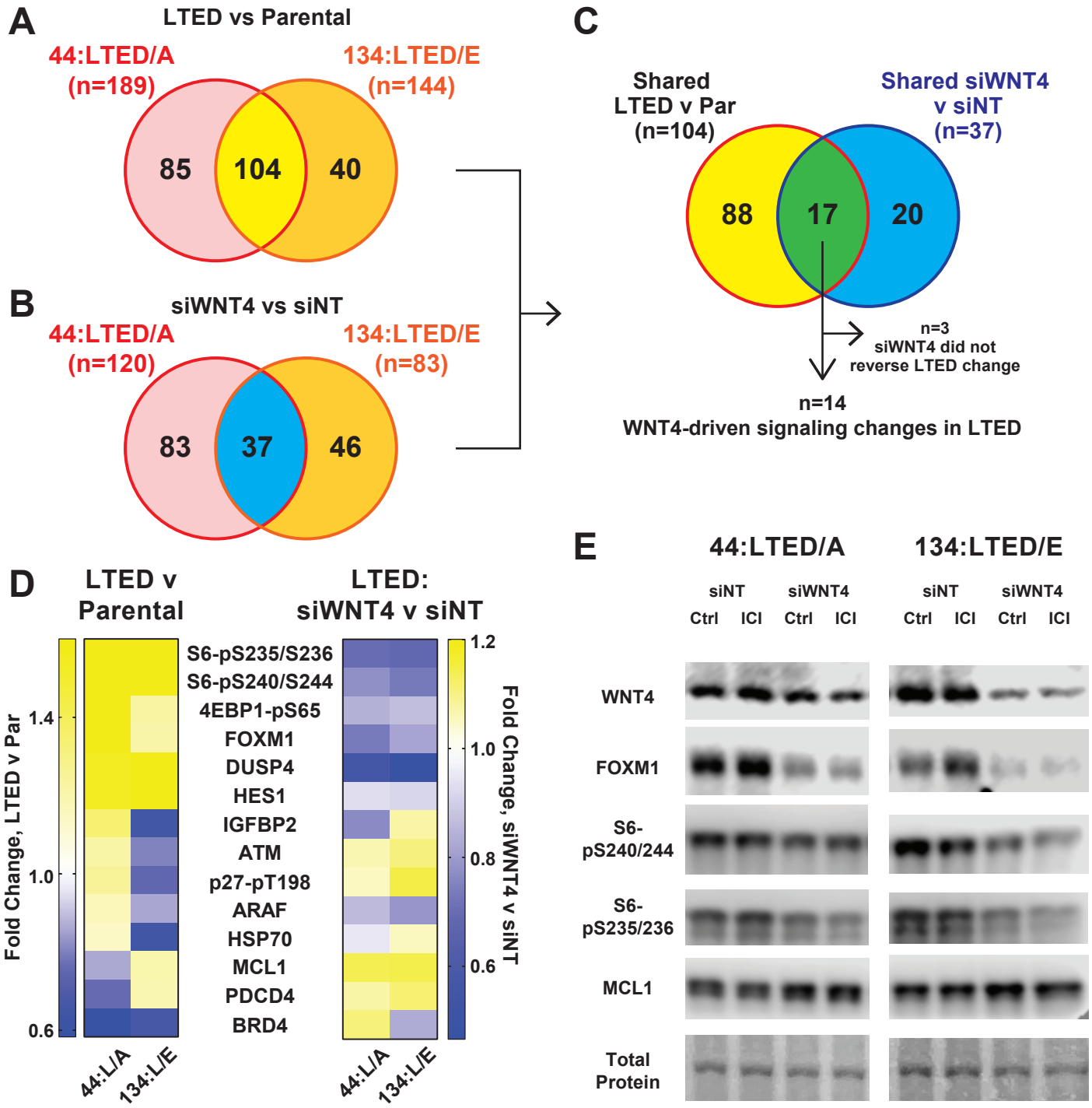
A
LTED vs Parental
44:LTED/A
(n=189)
134:LTED/E
(n=144)
85
104
40
B
siWNT4 vs siNT
44:LTED/A
(n=120)
134:LTED/E
(n=83)
83
37
46
C
Shared
LTED v Par
(n=104)
Shared siWNT4
v siNT
(n=37)
88
17
20
n=3
siWNT4 did not
reverse LTED change
n=14
WNT4-driven signaling changes in LTED
D
LTED v
Parental
LTED:
siWNT4 v siNT
Fold Change, LTED v Par
1.4
1.0
0.6
S6-pS235/S236
S6-pS240/S244
4EBP1-pS65
FOXM1
DUSP4
HES1
IGFBP2
ATM
p27-pT198
ARAF
HSP70
MCL1
PDCD4
BRD4
44:L/A
134:L/E
44:L/A
134:L/E
1.2
1.0
0.8
0.6
Fold Change, siWNT4 v siNT
E
44:LTED/A
134:LTED/E
siNT
siWNT4
siNT
siWNT4
Ctrl
ICI
Ctrl
ICI
Ctrl
ICI
Ctrl
ICI
WNT4
FOXM1
S6-
pS240/244
S6-
pS235/236
MCL1
Total
Protein

Figure 4. ER:WNT4 signaling targets are similarly active in anti-estrogen resistant ILC models. **A)** LTED cells were compared to their hormone-deprived (vehicle treated) parental cell line; differences at $q<0.05$ shown. **B)** LTED cells were reverse transfected with the indicated siRNA for 48hrs prior to harvest for RPPA analyses. RPPA protein signaling changes for siWNT4+E2 versus siNT+E2 shown ($p<0.05$). **C)** Overlap between signaling activation in LTED (from A) versus WNT4-driven signaling (from B) to identify specific WNT4-driven signaling that is activated during anti-estrogen resistance. For n=3, siWNT4 did not reverse the change seen in LTED v Parental in at least one of the two model systems. **D)** Heatmap of n=14 genes from (C) for LTED v Parental fold change (left) and siWNT4 v siNT fold change (right). Boxes show mean of biological triplicate samples. **E)** LTED cells (in hormone-deprivation) were reverse transfected with the indicated siRNA. 24hrs later, cells were treated with 1μM Fulv or vehicle, and lysates were harvested an additional 24hrs later.

FIGURE 5

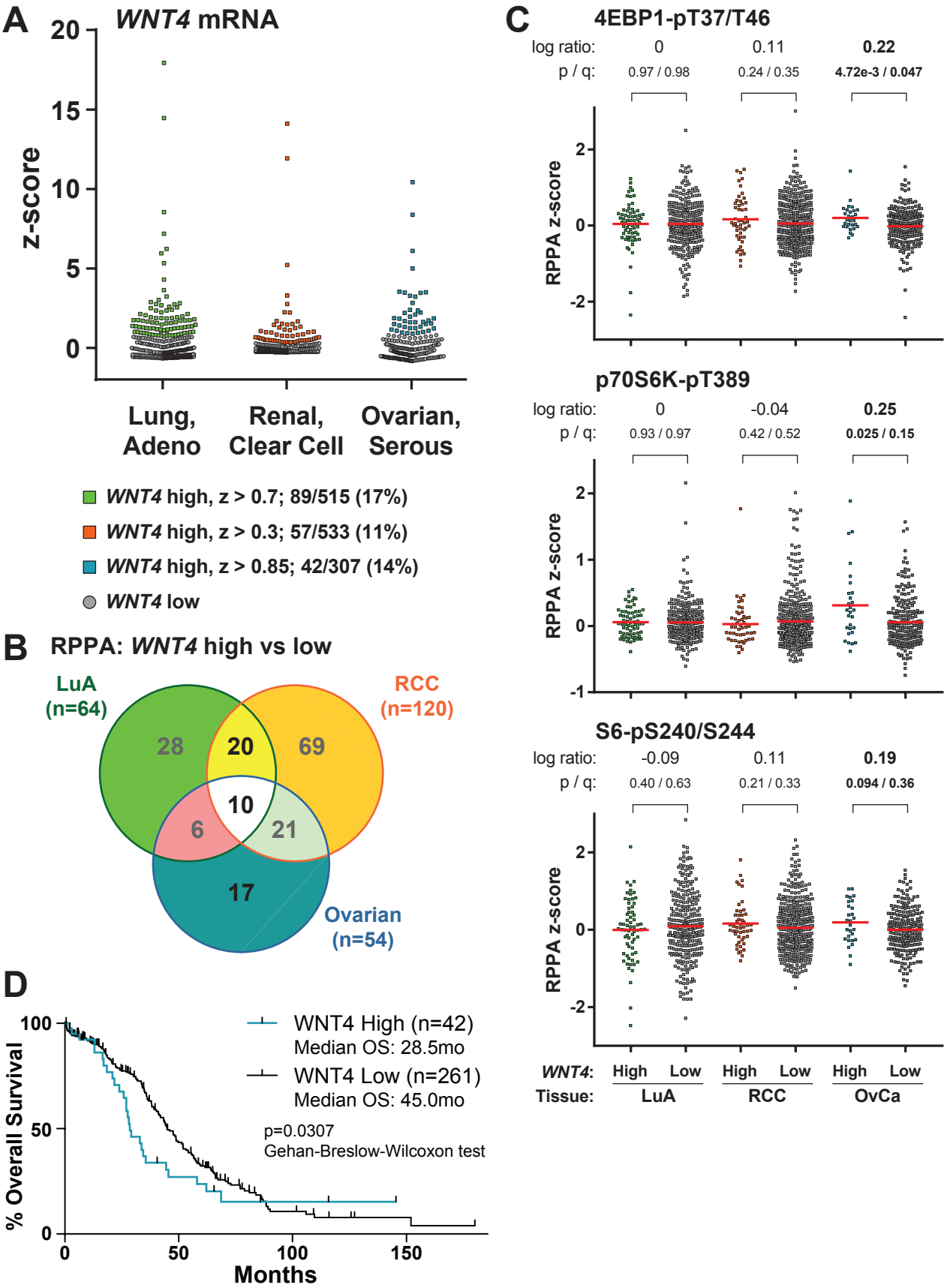
A
WNT4 mRNA
z-score
20
15
10
5
0
Lung, Adeno
Renal, Clear Cell
Ovarian, Serous
WNT4 high, z > 0.7; 89/515 (17%)
WNT4 high, z > 0.3; 57/533 (11%)
WNT4 high, z > 0.85; 42/307 (14%)
WNT4 low
B
RPPA: WNT4 high vs low
LuA (n=64)
RCC (n=120)
Ovarian (n=54)
28
20
69
10
6
21
17
C
4EBP1-pT37/T46
log ratio: 0 0.11 0.22
p / q: 0.97 / 0.98 0.24 / 0.35 4.72e-3 / 0.047
p70S6K-pT389
log ratio: 0 -0.04 0.25
p / q: 0.93 / 0.97 0.42 / 0.52 0.025 / 0.15
S6-pS240/S244
log ratio: -0.09 0.11 0.19
p / q: 0.40 / 0.63 0.21 / 0.33 0.094 / 0.36
RPPA z-score
WNT4: High Low High Low High Low
Tissue: LuA RCC OvCa
D
% Overall Survival
100
50
0
0
50
100
150
Months
WNT4 High (n=42)
Median OS: 28.5mo
WNT4 Low (n=261)
Median OS: 45.0mo
p=0.0307
Gehan-Breslow-Wilcoxon test

Figure 5. High *WNT4* expression is associated with activated mTOR signaling in serous ovarian cancer. A) RNAseq z-scores used to identify tumors with high *WNT4* mRNA levels in the indicated tumor types from TCGA data. Points represent individual tumor samples. **B)** cBio 'Enrichment' tool used to identify differences in RPPA signals ($p<0.1$) for high versus low *WNT4* levels. **C)** RPPA z-score for mTOR signaling components uniquely enriched in high *WNT4* OvCa samples. Colored v Gray points represent individual tumor samples with high/low *WNT4* from (A). Line represents mean RPPA signal for the indicate group. Log ratio shown as High v Low *WNT4*. **D)** Overall survival data derived from cBio 'Survival' tool. High v Low *WNT4* as in (A).

SUPPLEMENTAL FIGURE 1

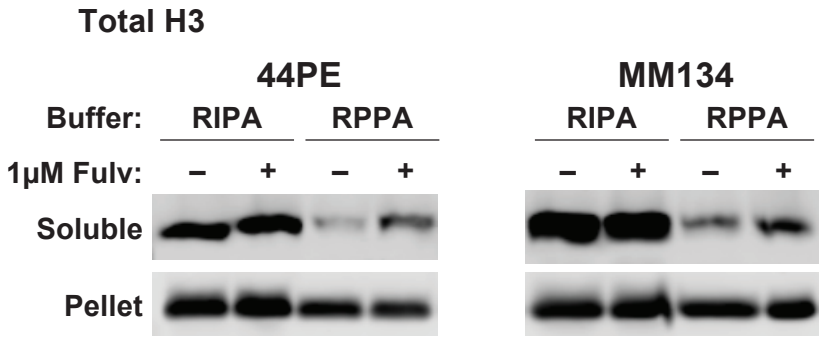

Supplemental Figure 1. Histone H3 signal on RPPA represents the soluble histone pool. ILC cells were treated with Fulvestrant or vehicle for 24hrs and lysed with either RPPA buffer (as described in Materials and Methods) or RIPA buffer. RPPA buffer (lacks SDS) does not solubilize compacted chromatin, which is pelleted and removed prior to further processing (ie. pellet sample, which contains most of the cellular pool of histones).

SUPPLEMENTAL FIGURE 2

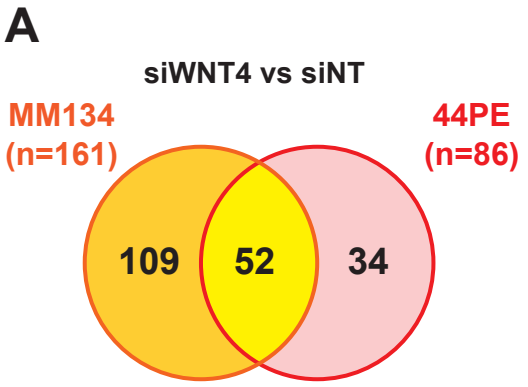

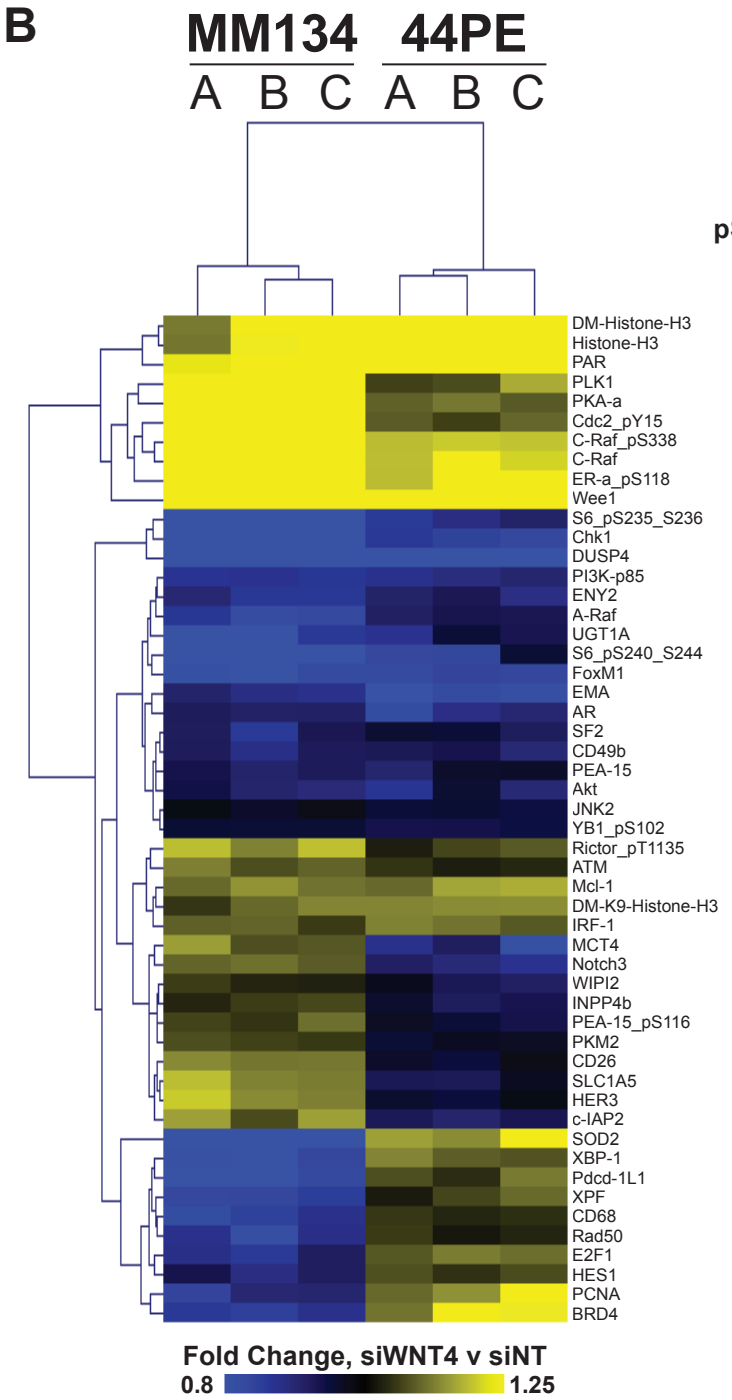

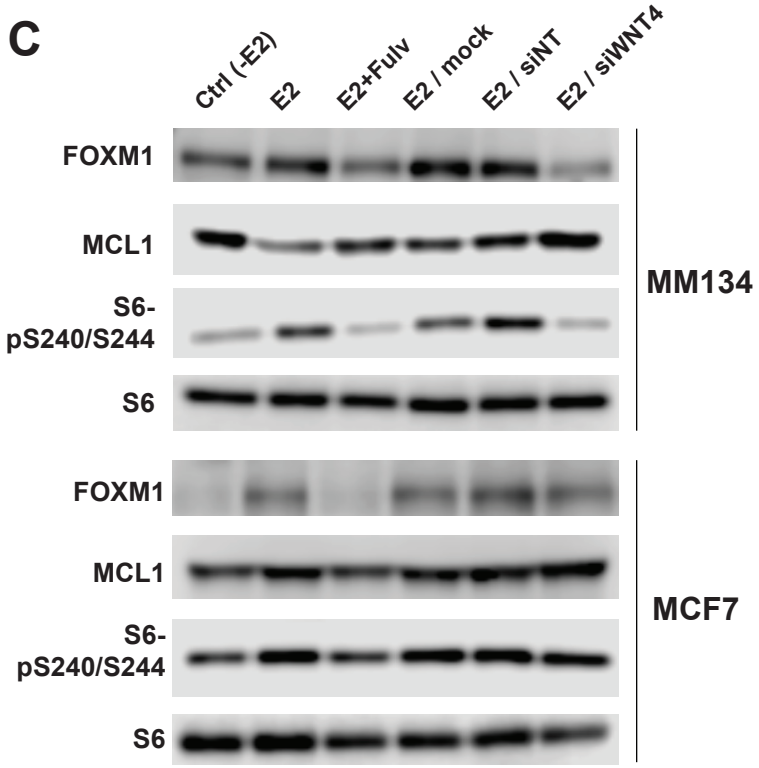

Supplemental Figure 2. WNT4 knockdown broadly affects signaling in ILC cells. A) Cells were hormone-deprived prior to siRNA reverse transfection and subsequent treatment with 100pM E2 for 24hrs (biological triplicate; see Materials and Methods). RPPA protein signaling changes for siWNT4+E2 versus siNT+E2 shown ($p<0.05$). **B)** Heatmap for shared targets, siWNT4 vs siNT. A/B/C represent biological replicate samples. **C)** Cells were treated and transfected as in (A).

SUPPLEMENTAL FIGURE 3

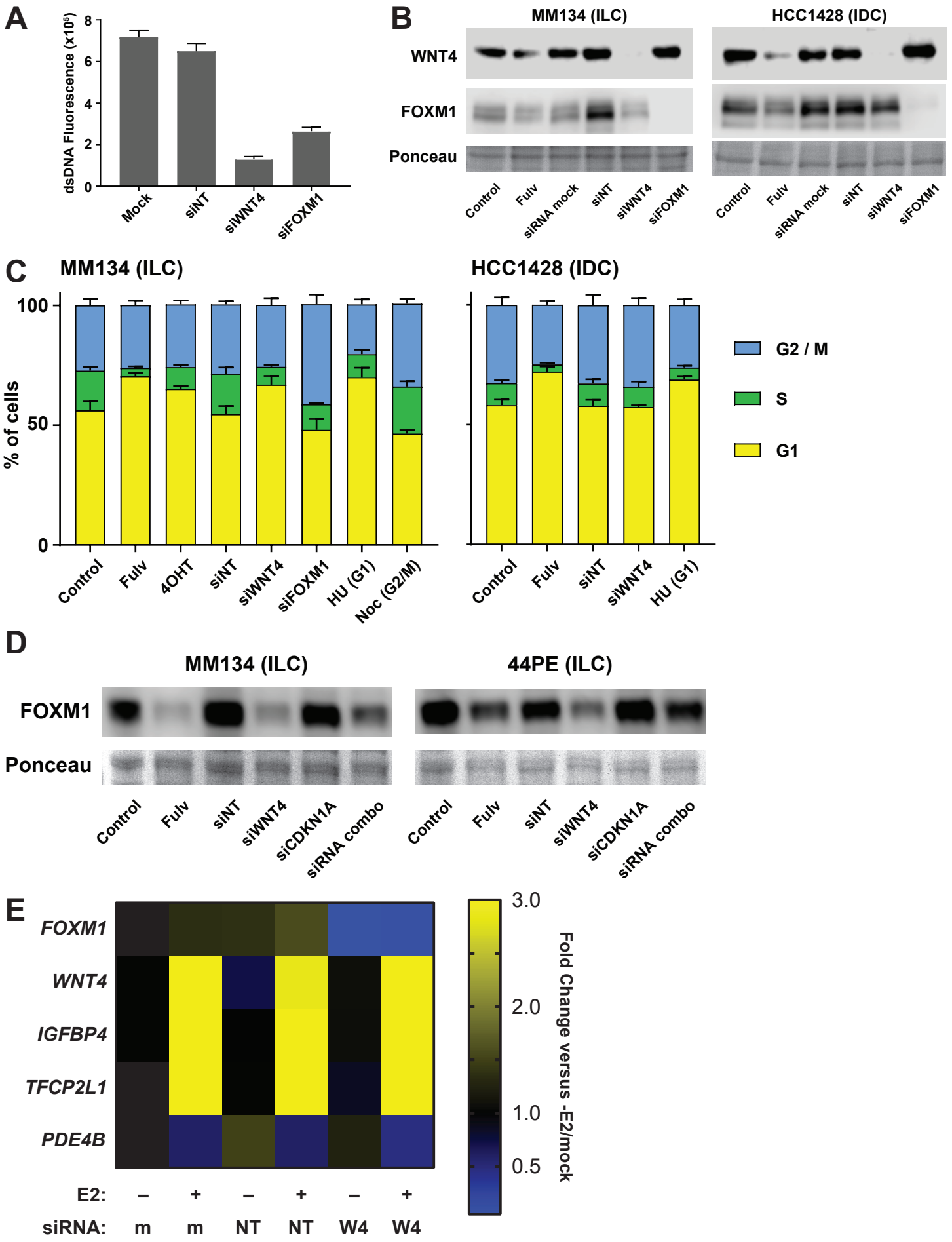

Supplemental Figure 3. FOXM1 is not a direct target of WNT4 signaling. A) MM134 cells in full serum were reverse transfected with the indicated siRNA, and proliferation was assessed by dsDNA quantification after 6d. Bars represent mean of 6 biological replicates ±SD. **B)** Confirmation of WNT4 or FOXM1 knockdown. MM134 cells in full serum were reverse transfected with the indicated siRNA. 24hrs later, cells were treated with Fulv, and lysates were harvested an additional 24hrs later. **C)** Cells in full serum were transfected and treated as in (B) using 1μM Fulvestrant, 1μM 4-hydroxytamoxifen, 2mM hydroxyurea, or 50ng/mL nodocazole. Bars represent mean cell fraction per cell cycle phase of 3 biological replicate experiments ±SD. **D)** Cells were transfected and treated as in (B). In siRNA combinations, siNT was used to increase total siRNA to 20nM in single siRNA samples. **E)** Hormone-deprived MM134 were reverse transfected with the indicated siRNA. 24hrs later, cells were treated with 100pM E2 or vehicle, and RNA was harvested an additional 24hrs later. Expression was normalized to *RPLP0*. Box represents mean fold change of biological triplicate samples, versus the –E2/mock control sample (Column 1).

SUPPLEMENTAL FIGURE 4

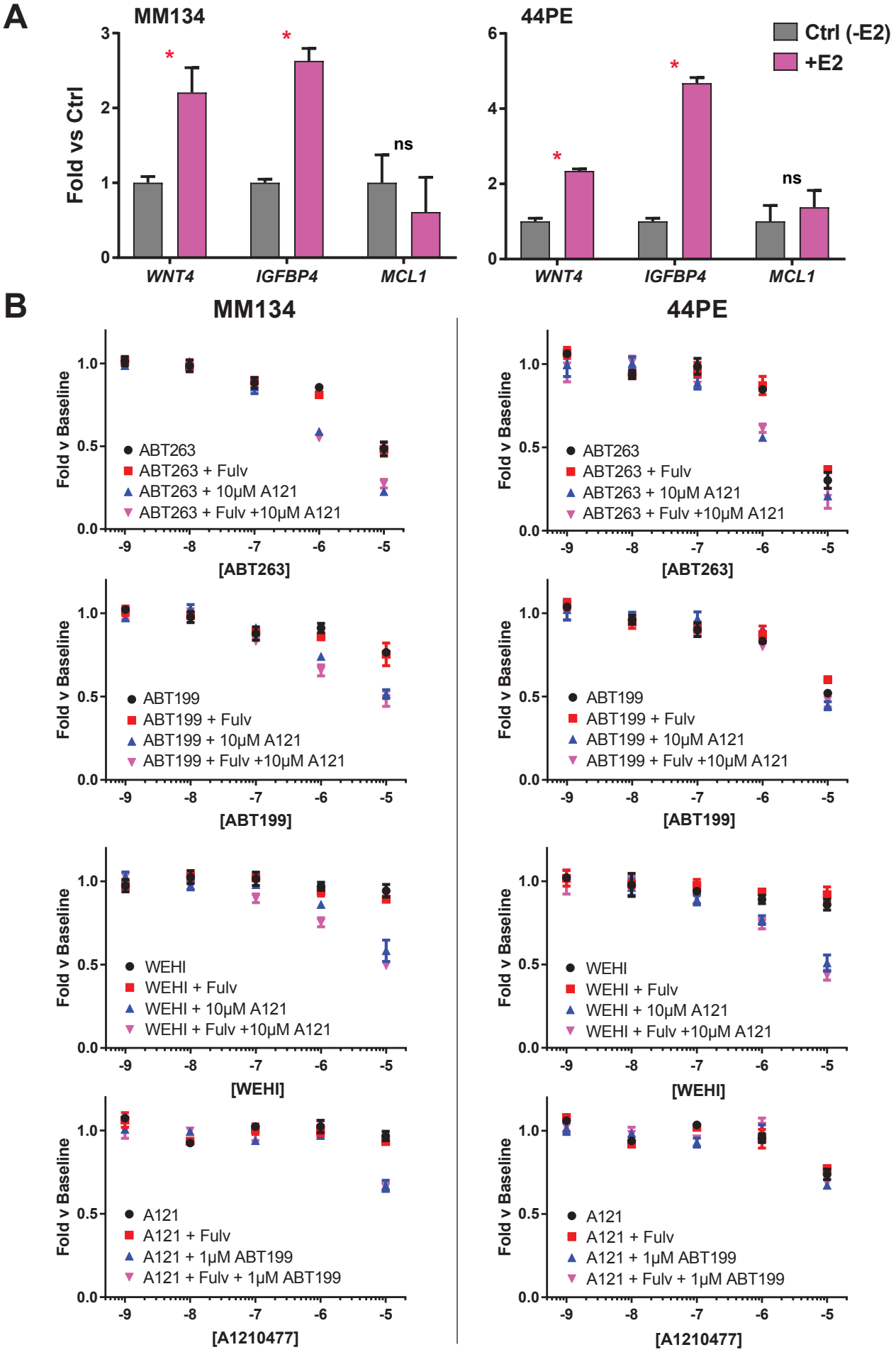

Supplemental Figure 4. ER regulation of MCL-1 is not linked to shifts in sensitivity to BH3 mimetic drugs. A) Cells were hormone-deprived prior to siRNA reverse transfection and subsequent treatment with 100pM E2 for 24hrs. Expression was normalized to *RPLP0*. *, Ctrl vs +E2, $p < 0.05$, Student's T-test. **B)** Cells in full serum were pre-treated with 100nM fulvestrant and/or base BH3 mimetic (ie. the compound at static concentration per assay) for 6 hours prior to treatment with increasing concentrations of the test BH3 mimetic. Cell proliferation/death was assessed by dsDNA quantification 72hrs after second treatment. Points represent mean of biological triplicate ±SD.

SUPPLEMENTAL FIGURE 5

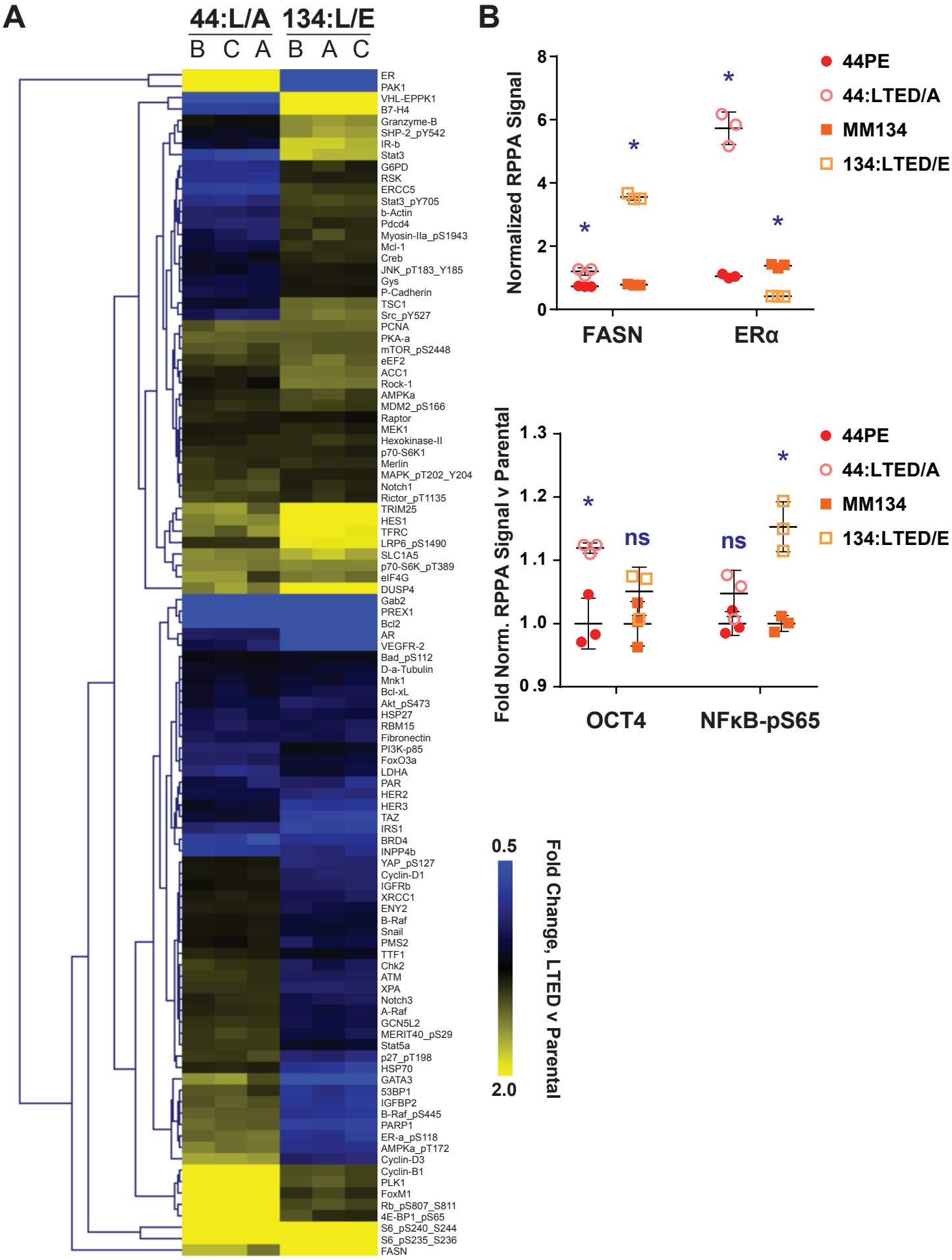

Supplemental Figure 5. RPPA identifies diverse signaling pathways activated during anti-estrogen resistance in ILC models. A) Heatmap for n=104 shared protein signaling changes for LTED versus parental cells. A/B/C represent biological replicate samples. **B)** Protein changes in LTED models that support previously described features of the anti-estrogen resistance phenotype in these models. Points represent individual biological replicates. *, Matched parental v LTED, $q<0.05$.

SUPPLEMENTAL FIGURE 6

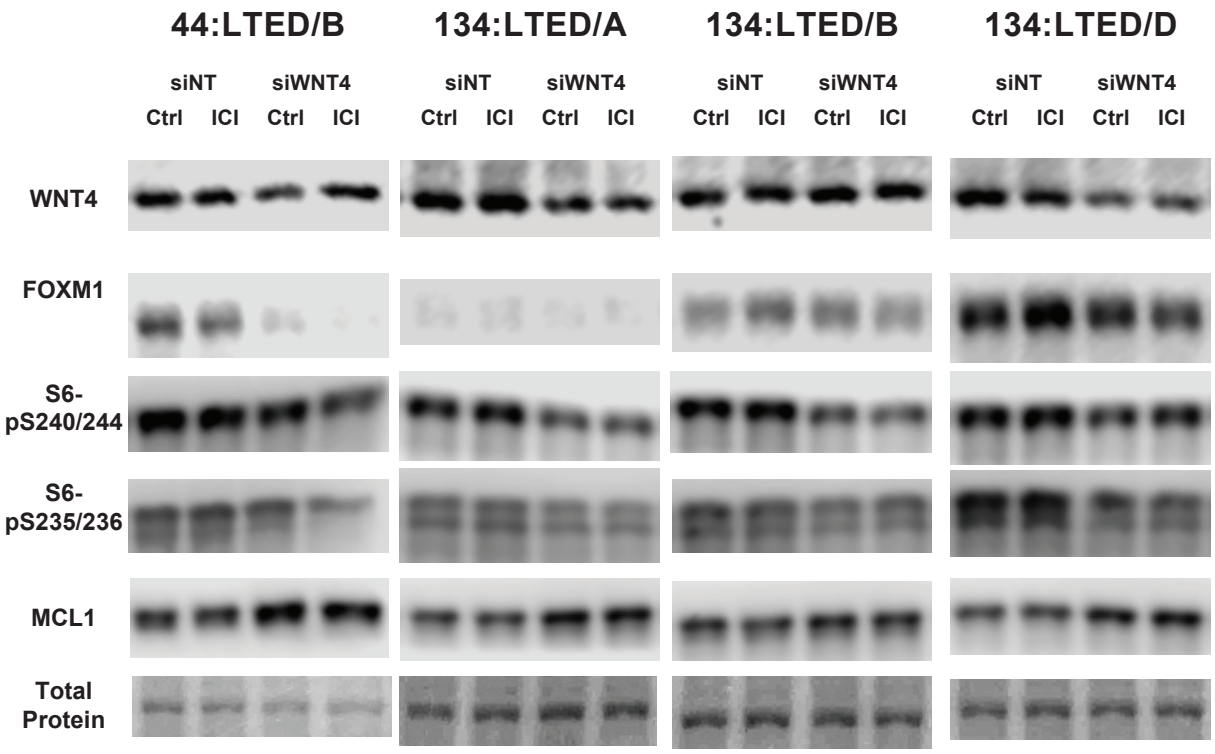

Supplemental Figure 6. WNT4 regulation of key targets is consistent across ILC LTED cell lines. LTED cells (in hormone-deprivation) were reverse transfected with the indicated siRNA. 24hrs later, cells were treated with 1μM Fulv or vehicle, and lysates were harvested an additional 24hrs later.

SUPPLEMENTAL FIGURE 7

A

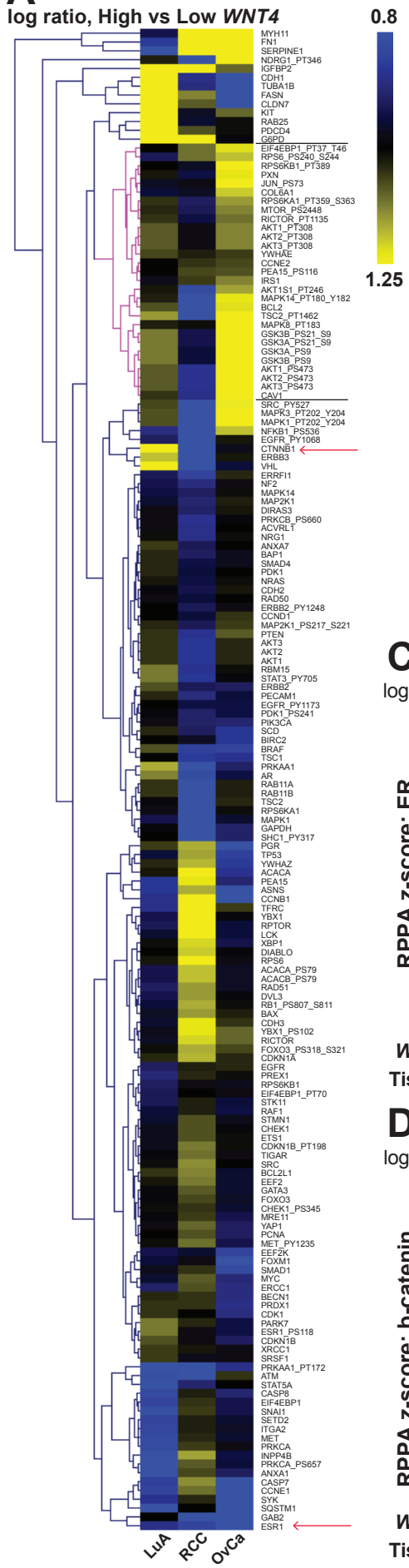

B Ovarian (Serous) RPPA, High vs Low *WNT4* mRNA

Gene	Log Ratio	p-Value	q-Value
GSK3A_PS9	0.45	3.09E-08	**3.20E-06**
GSK3B_PS9	0.45	3.09E-08	**3.20E-06**
CASP7	-0.42	3.00E-06	**2.07E-04**
TSC2_PT1462	0.29	1.31E-05	**4.71E-04**
GSK3A_PS21_S9	0.33	1.37E-05	**4.71E-04**
GSK3B_PS21_S9	0.33	1.37E-05	**4.71E-04**
SMAD1	-0.22	5.76E-05	**1.70E-03**
CCNE1	-0.43	1.82E-04	**4.71E-03**
SYK	-0.49	5.31E-04	**0.0106**
MAPK8_PT183	0.36	6.40E-04	**0.0106**
AKT1_PS473	0.46	6.65E-04	**0.0106**
AKT2_PS473	0.46	6.65E-04	**0.0106**
AKT3_PS473	0.46	6.65E-04	**0.0106**
SQSTM1	-0.55	8.18E-04	**0.0121**
GAB2	-0.4	1.86E-03	**0.0256**
RPS6KA1_PT359_S363	0.15	2.10E-03	**0.0271**
EEF2K	-0.2	3.05E-03	**0.0368**
JUN_PS73	0.25	3.20E-03	**0.0368**
CLDN7	-0.62	4.22E-03	**0.0459**
EIF4EBP1_PT37_T46	0.22	4.72E-03	**0.0468**
BIRC2	-0.17	4.75E-03	**0.0468**
ERCC1	-0.14	5.12E-03	**0.0482**
MYH11	1.19	6.65E-03	0.0599
CASP8	-0.12	8.30E-03	0.0716
PXN	0.23	0.0108	0.0892
BCL2	0.22	0.0144	0.111
ASNS	-0.26	0.0145	0.111

Gene	Log Ratio	p-Value	q-Value
MTOR_PS2448	0.13	0.0195	0.144
NDRG1_PT346	0.39	0.0208	0.147
AKT1S1_PT246	0.16	0.0215	0.147
PIK3CA	-0.12	0.0221	0.147
EGFR_PY1173	-0.07	0.0238	0.147
PRDX1	-0.15	0.0243	0.147
PRKAA1	-0.11	0.0248	0.147
RPS6KB1_PT389	0.25	0.0249	0.147
MAPK14_PT180_Y182	0.23	0.0268	0.154
FOXM1	-0.25	0.036	0.197
CDK1	-0.14	0.0369	0.197
YWHAZ	-0.18	0.0379	0.197
ESR1	-0.54	0.0388	0.197
RICTOR_PT1135	0.11	0.039	0.197
BRAF	-0.2	0.0431	0.213
CAV1	0.46	0.0488	0.235
PCNA	-0.1	0.0562	0.264
IRS1	0.13	0.0574	0.264
CCNB1	-0.35	0.0597	0.265
CDH1	-0.44	0.061	0.265
BECN1	-0.14	0.0615	0.265
COL6A1	0.2	0.0747	0.316
FASN	-0.27	0.0804	0.333
MYC	-0.13	0.0828	0.336
PEA15	-0.12	0.0918	0.359
SRC_PY527	0.24	0.092	0.359
RPS6_PS240_S244	0.19	0.0943	0.362

C ERα

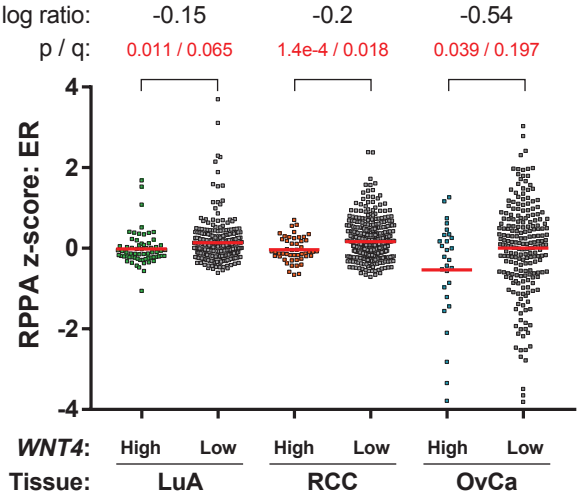

D β-catenin

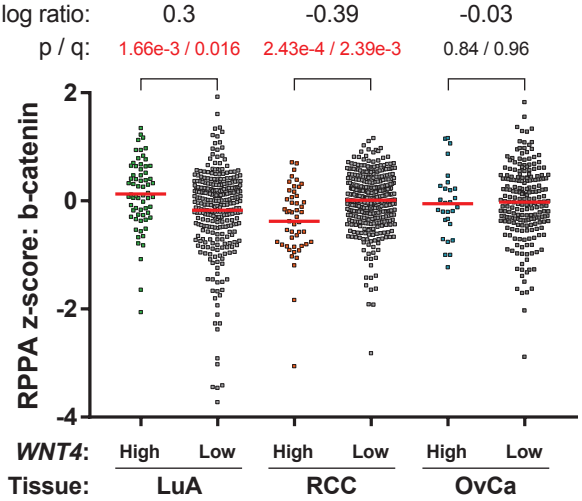

E

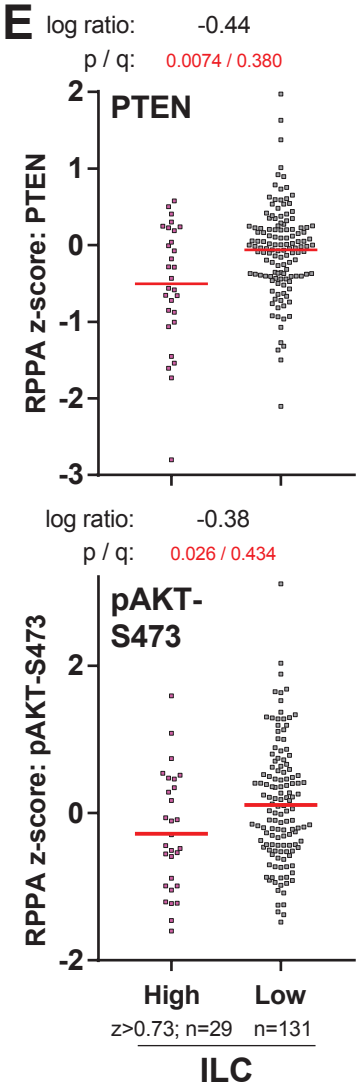

Supplemental Figure 7. High *WNT4* expression is associated with distinct signaling pathways in varying tumor types. A) TCGA RPPA data from Figure 5B; n=170 protein targets different in high v low *WNT4*-expressing tumors in at least one tumor type at $p<0.1$. Brackets identify mTOR signaling targets increased only in OvCa; arrows denote targets in (C-D). **B)** All protein target changes in OvCa in high v low *WNT4*-expressing tumors at $p<0.1$; bold denotes $q<0.05$. **C-D)** RPPA z-score for shared signaling components discussed in text. Colored v Gray points represent individual tumor samples with high/low *WNT4* from (A). Line represents mean RPPA signal for the indicate group. Log ratio shown as High v Low *WNT4*. **E)** No protein signals at $q<0.05$ were identified in *WNT4* high v low expressing ILC; PTEN and pAKT-S473 were included among n=17 differentially expressed protein targets at $p<0.05$. Colored v Gray points represent individual tumor samples with high/low *WNT4*.